WILEY

RESEARCH ARTICLE

Aspergillus fumigatus protein phosphatase PpzA is involved in iron assimilation, secondary metabolite production, and virulence

Adriana Oliveira Manfiolli[1] | Patrícia Alves de Castro[1] | Thaila Fernanda dos Reis[1] | Stephen Dolan[2] | Sean Doyle[2] | Gary Jones[2] | Diego M. Riaño Pachón[3] | Mevlüt Ulaş[2] | Luke M. Noble[4] | Derek J. Mattern[5,6] | Axel A. Brakhage[5,6] | Vito Valiante[7] | Rafael Silva-Rocha[8] | Ozgur Bayram[2] | Gustavo H. Goldman[1] iD

[1] Faculdade de Ciências Farmacêuticas de Ribeirão Preto, Universidade de São Paulo, Ribeirão Preto, Brazil

[2] Department of Biology, Maynooth University, Maynooth, Co. Kildare, Ireland

[3] Laboratório Nacional de Ciência e Tecnologia do Bioetanol (CTBE), Centro Nacional de Pesquisa em Energia e Materiais (CNPEM), Campinas, São Paulo, Brazil

[4] New York University, New York, NY, USA

[5] Department of Molecular and Applied Microbiology, Leibniz Institute for Natural Product Research and Infection Biology—Hans Knöll Institute, Jena, Germany

[6] University of Jena, Jena, Germany

[7] Leibniz Research Group—Biobricks of Microbial Natural Product Syntheses, Leibniz Institute for Natural Product Research and Infection Biology—Hans Knöll Institute, Jena, Germany

[8] Faculdade de Medicina de Ribeirão Preto, Universidade de São Paulo, Ribeirão Preto, Brazil

Correspondence
Gustavo H. Goldman, Faculdade de Ciências Farmacêuticas de Ribeirão Preto, Universidade de São Paulo, Ribeirão Preto, Brazil.
Email: ggoldman@usp.br

Ozgur Bayram, Department of Biology, Maynooth University, Maynooth, Co. Kildare, Ireland.
Email: ozgur.bayram@nuim.ie; ozgur.bayram@mu.ie

Summary

Metal restriction imposed by mammalian hosts during an infection is a common mechanism of defence to reduce or avoid the pathogen infection. Metals are essential for organism survival due to its involvement in several biological processes. *Aspergillus fumigatus* causes invasive aspergillosis, a disease that typically manifests in immunocompromised patients. *A. fumigatus* PpzA, the catalytic subunit of protein phosphatase Z (PPZ), has been recently identified as associated with iron assimilation. *A. fumigatus* has 2 high-affinity mechanisms of iron acquisition during infection: reductive iron assimilation and siderophore-mediated iron uptake. It has been shown that siderophore production is important for *A. fumigatus* virulence, differently to the reductive iron uptake system. Transcriptomic and proteomic comparisons between *ppzA* and wild-type strains under iron starvation showed that PpzA has a broad influence on genes involved in secondary metabolism. Liquid chromatography-mass spectrometry under standard and iron starvation conditions confirmed that the Δ*ppzA* mutant had reduced production of pyripyropene A, fumagillin, fumiquinazoline A, triacetyl-fusarinine C, and helvolic acid. The Δ*ppzA* was shown to be avirulent in a neutropenic murine model of invasive pulmonary aspergillosis. PpzA plays an important role at the interface between iron starvation, regulation of SM production, and pathogenicity in *A. fumigatus*.

1 | INTRODUCTION

The saprophytic fungus *Aspergillus fumigatus* grows in soil and organic debris (Latgé, 1999), where it is responsible for organic material recycling (Tekaia & Latge, 2005). *A. fumigatus* causes invasive aspergillosis (IA), a disease that typically manifests in immunocompromised patients. Hundreds of *A. fumigatus* conidia are inhaled daily and, in immune competent hosts, are killed and removed by cells of the pulmonary immune system. In contrast, in immunocompromised patients, conidia can germinate and penetrate epithelial and endothelial

barriers (Hohl & Feldmesser, 2007). IA incidence has increased alongside medical practices such as immunosuppression in transplant patients and aggressive anticancer chemotherapy, which predisposes patients to IA. Mortality attributed to IA infections caused by *Aspergillus* species range from 60% to 90%, depending on the type of infectious event (Brakhage, 2005; Tekaia & Latge, 2005). Some biological processes are known to be important for the infection, such as the following: the composition of the cell wall, hypoxia tolerance, gliotoxin production, thermophily, and iron assimilation (Dagenais & Keller, 2009). Furthermore, *A. fumigatus* can generate hundreds of secondary metabolites (SMs) that are bioactive small molecules. Commonly, the genes involved in SM production are clustered and subjected to common regulatory patterns (Brakhage, 2013; Frisvad, Rank, Nielsen, & Larsen, 2009; Hoffmeister & Keller, 2007; Macheleidt et al., 2016). It has been related that some of these SMs are involved and contribute to fungal virulence (Bok et al., 2006; Heinekamp et al., 2012; Yin et al., 2013).

Aspergillus fumigatus PpzA, the catalytic subunit of protein phosphatase Z (PPZ), has been recently identified as associated with iron assimilation (Winkelströter et al., 2015). Null *ppzA* mutants have reduced biomass accumulation upon iron starvation conditions (Winkelströter et al., 2015). The gene *ppzA* is regulated by the Skn7 transcription factor, and it is involved in corneal infection by *A. fumigatus* (Muszkieta *et al.*, 2014). Iron functions as an important cofactor in many cellular processes and is an essential nutrient. Iron binds to several proteins involved in essential cellular processes, such as gene regulation; the tricarboxylic acid cycle; respiration; and amino acid, deoxyribonucleotide, and lipid biosynthesis (Cairo, Bernuzzi, & Recalcati, 2006). Moreover, it is also known that the control of the iron access is crucial for the success of microbial infection in mammalian host and iron deficiency is important for regulation of virulence in other microorganisms (Litwin & Calderwood, 1993; Oglesby-Sherrouse, Djapgne, Nguyen, Vasil, & Vasil, 2014; Weinberg, 2009).

Aspergillus fumigatus has two high-affinity mechanisms of iron acquisition during infection: reductive iron assimilation (RIA) and siderophore-mediated iron uptake (Schrettl & Haas, 2011; Schrettl et al., 2004). Siderophores are nonribosomal peptide and iron-specific chelators (Haas, 2003). Two of them, fusarinine C and triacetyl-fusarinine C, are secreted to capture extracellular iron. Their ferri-forms are imported by siderophore-iron transporters and hydrolysed intracellularly releasing the imported iron. The presence of intracellular siderophores is a particular feature of fungi (Schrettl & Haas, 2011). *A. fumigatus* has two intracellular siderophores: conidial hydroxyferricrocin and hyphal ferricrocin. These intracellular siderophores are responsible for distribution and storage of iron (Oberegger, Schoeser, Zadra, Abt, & Haas, 2001; Schrettl et al., 2007; Wallner et al., 2009). RIA is performed by plasma membrane-localised ferrireductase associated to iron permease and oxidase. This process starts with reduction of iron, then the ferrous iron obtained is re-oxidised and taken up by a protein complex comprising iron permease FtrA and ferroxidase FetC (Kosman, 2013). It has been shown that siderophore production is significant for *A. fumigatus* virulence, differently to the reductive iron uptake system (Eisendle, Oberegger, Zadra, & Haas, 2003; Gauthier *et al.*, 2010; Greenshields, Liu, Feng, Selvaraj, & Wei, 2007; Hissen, Wan, Warwas, Pinto, & Moore, 2005; Hwang, Grouph, Gilmore, & Sil, 2012; Oide et al., 2006; Schrettl et al., 2004, 2007).
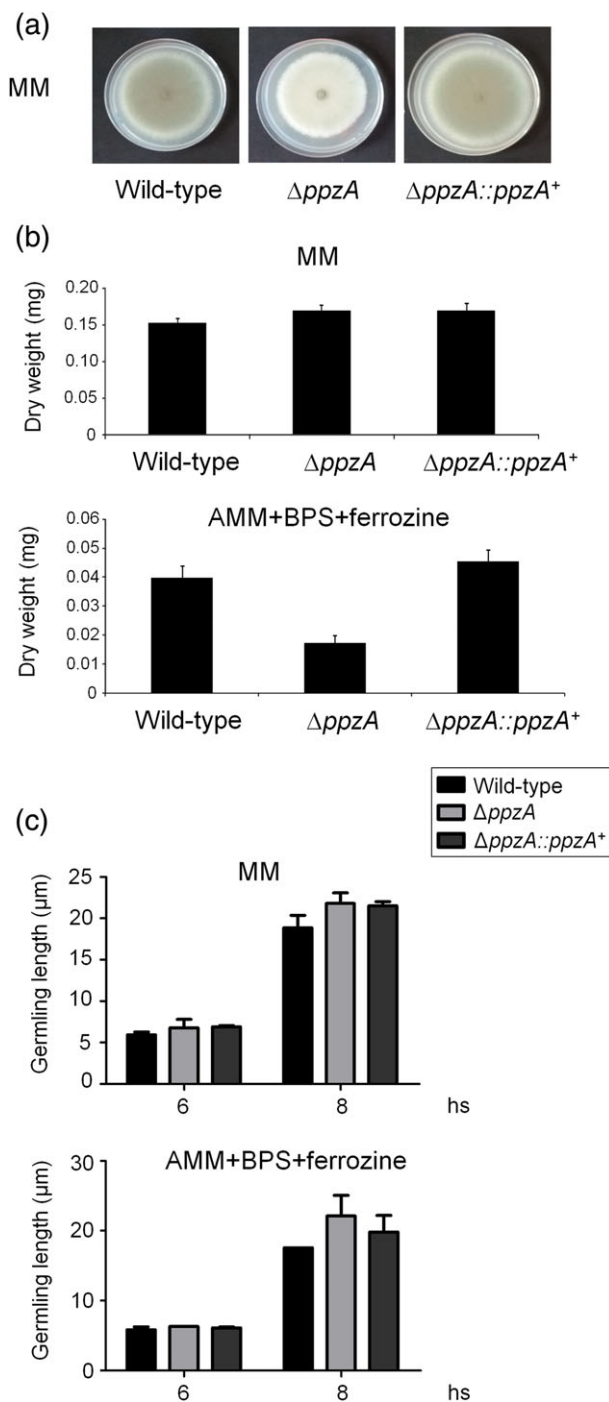
Additionally, homeostasis of cellular iron is closely regulated to ensure the balance among uptake, storage, and consumption of iron and avoid toxic iron excess, because iron presents a dual role in organismal physiology. In fungi, homeostasis of metal ions is maintained mainly through transcriptional regulation of gene expression. A group of transcription factors of the GATA type, which are iron responsive, mediates gene repression for the acquisition of this micronutrient when it is available in sufficient concentrations (Rutherford & Bird, 2004). These factors have already been described in *Cryptococcus neoformans* (Cir1, also acting as an activator of genes involved in siderophore uptake), *Histoplasma capsulatum* (Sre1), *Blastomyces dermatitidis* (SreB), *Candida albicans* (Sfu1), and *A. fumigatus* (SreA; Gauthier *et al.*, 2010; Jung & Kronstad, 2008; Lan, Rodarte, Murillo, et al., 2004; Schrettl, Kim, Eisendle, et al., 2008). However, the response to low iron concentrations is mediated by a bZIP-type regulator (Hortschansky et al., 2007). In *A. fumigatus*, HapX suppresses pathways that depend on iron, such as respiration, haem biosynthesis, and the tricarboxylic acid cycle, during the absence of this nutrient, whereas siderophore-mediated iron uptake is induced. Thus, GATA and bZIP-type regulators act in opposite ways depending on iron availability in the environment. However, HapX is also pivotal for iron resistance because it activated vacuolar iron storage (Gsaller et al., 2014). Furthermore, HapX is involved in fungal virulence in *A. fumigatus* and *Fusarium oxysporum*, corroborating the important role of siderophores production for the establishment of full virulence (Schrettl et al., 2010).

Considering the significance of iron metabolism in the fungus, together with the putative iron assimilation role of the protein phosphatase PpzA, we aimed to characterise the importance of PpzA in iron-dependent regulation in *A. fumigatus*. To gain a comprehensive insight into the pathways that are modulated by this phosphatase, we performed transcriptomic and proteomic analyses comparing the corresponding wild-type strain with the *ppzA* mutant under iron replete and starvation conditions. In addition to genes encoding transporters, oxidoreductases, and transcription factors, enzymes that participate in the biosynthesis of SMs, such as neosartoricin/fumicycline, gliotoxin, endocrocin, and fumagillin, were differentially expressed in the mutant strain. Furthermore, siderophore biosynthetic machinery components, enzymes involved in SM production, and the alternative oxidase (AoxA), which is transcriptionally induced in response to oxidative stress, were increased at translational level in *ΔppzA* under iron starvation. Finally, *ΔppzA* was avirulent in a low-dose murine infection model. on the basis of our data, we propose that PpzA plays an important role in posttranslational alterations involved in the iron-dependent secondary metabolism network.

2 | RESULTS

2.1 | Transcriptome analysis comparing the wild type and *ΔppzA* under iron starvation

As previously shown (Winkelströter *et al.*, 2015), *A. fumigatus ΔppzA* has comparable growth to the wild-type and complementing strains in minimal media (MM, Figure 1a,b); however, it has reduced growth when grown in iron starvation conditions (Figure 1b). The iron chelating agents used here, BPS

FIGURE 1 The Δ*ppzA* mutant has reduced growth in iron starvation conditions. (a) The wild type and Δ*ppzA* were grown for 96 hr at 37 °C in solid MM. (b) The wild type and Δ*ppzA* were grown for 48 hr at 37 °C in liquid MM or AMM + BPS + ferrozine. (c) Germling length (μm) of the wild-type and Δ*ppzA* strains grown for 6 and 8 hr in liquid MM or AMM + BPS + ferrozine

[200 μM, bathophenanthrolinedisulfonic acid (4,7-diphenyl-1,10 phenanthrolinedisulfonic acid)] and ferrozine [300 μM, 3-(2-pyridyl)-5,6-bis(4-phenylsulfonic acid)-1,2,4-triazine], have been extensively used for iron assimilation studies in *A. fumigatus* (Schrettl & Haas, 2011; Schrettl et al., 2004). The growth length and emergence of the germlings and the number of nuclei/germlings are not statistically different among the wild-type, Δ*ppzA*, and Δ*ppzA::ppzA⁺* strains (Figure 1c and S1, data not shown). To describe how

A. fumigatus wild-type strain responds and adapts to iron starvation, we evaluated the genome-wide transcriptional profile by RNA-seq. We defined differentially expressed genes as those with a minimum of twofold change in gene expression (controlling at an false discovery rate (FDR) of 0.05) when compared to the unstressed equivalent of the same strain (control, 0 min; Tables S1 and S2). After 1 hr of iron starvation, 1,264 and 1,390 genes were upregulated and downregulated in the wild-type strain, respectively. Moreover, 1,011 and 1,035 genes were upregulated and downregulated in the wild-type strain, respectively, after 2 hr of iron starvation. The results are summarised in detail in Table S1. Gene Ontology (GO) enrichment analyses of the differentially expressed genes in the wild type showed a transcriptional upregulation of nucleotide metabolic process, transcription from RNA polymerase I promoter, and ribosome biogenesis (Table 1). As expected, the bZip-factor HapX and genes related to siderophore biosynthesis and reductive iron uptake were found to be upregulated after iron starvation. Genes identified in these categories encode *sidI*, *sidF*, *sidD*, *sidH*, *sidG*, *sidA*, *sidC*, and the metalloreductase-encoding gene *fre2*, the putative ferric chelate reductase-encoding gene *fre7*, and the putative high-affinity iron permease *frtA* (Tables S1 and S2). Some of the downregulated genes identified are involved in oxidation–reduction processes, mitochondrial electron transport, and response to oxidative and osmotic stress (Table 1). Furthermore, some important genes involved in SM production were also found to be differentially expressed. Among them, a polyketide synthase (PKS) encoded in the neosartoricin/fumicycline SM gene cluster, a brevianamide F prenyltransferase involved in the biosynthesis of fumitremorgins, a oxidoreductase involved in endocrocin biosynthesis, and the nonribosomal peptide synthetase (NRPS) genes *pesG*, *pesB*, and *ftmA* were upregulated in the wild type after iron starvation. Interestingly, a flavin-dependent monooxygenase and the pathway-specific $Zn(II)_2Cys_6$ transcriptional factor, encoded within the neosartoricin/fumicycline SM gene cluster, as well as an NRPS required for pseurotin A production were significantly downregulated (Tables S1 and S2).

Because previous results revealed that *ppzA* showed a reduced growth in iron starvation conditions (Winkelströter et al., 2015), RNA-sequencing was used to identify targets modulated directly or indirectly by PpzA. We did a global analysis of genes that are regulated by PpzA under iron starvation and compared it with the previous analysis in the wild-type strain. Once more, we defined the differentially expressed genes as those with a minimum of twofold change in gene expression (controlling at an FDR of 0.05) when comparing the mutant to the wild-type strain. In *ppzA*, 80 and 17 genes were upregulated and downregulated after 1 hr of iron starvation, respectively, compared to the wild type (Figure 2a). After 2 hr of starvation, compared to the wild type, 73 and 55 genes were upregulated and downregulated, respectively (Figure 2a). A common group of 30 and 2 genes upregulated and downregulated, respectively, were identified between the two comparisons (Figure 2a). Enrichment analysis of the differentially expressed genes in *ppzA* showed both upregulation and downregulation of biological categories such as transcription factor, secondary metabolism, transporters, and oxidoreductase activity (Figure 2b-e and Tables S3 and S4). The Δ*ppzA* showed a transcriptional upregulation of genes involved in transporter activity, such as MFS gliotoxin

TABLE 1 A summary of the GO terms over-represented upregulated or downregulated in log2FC wild-type post transfer to iron starvation for 1 or 2 hr

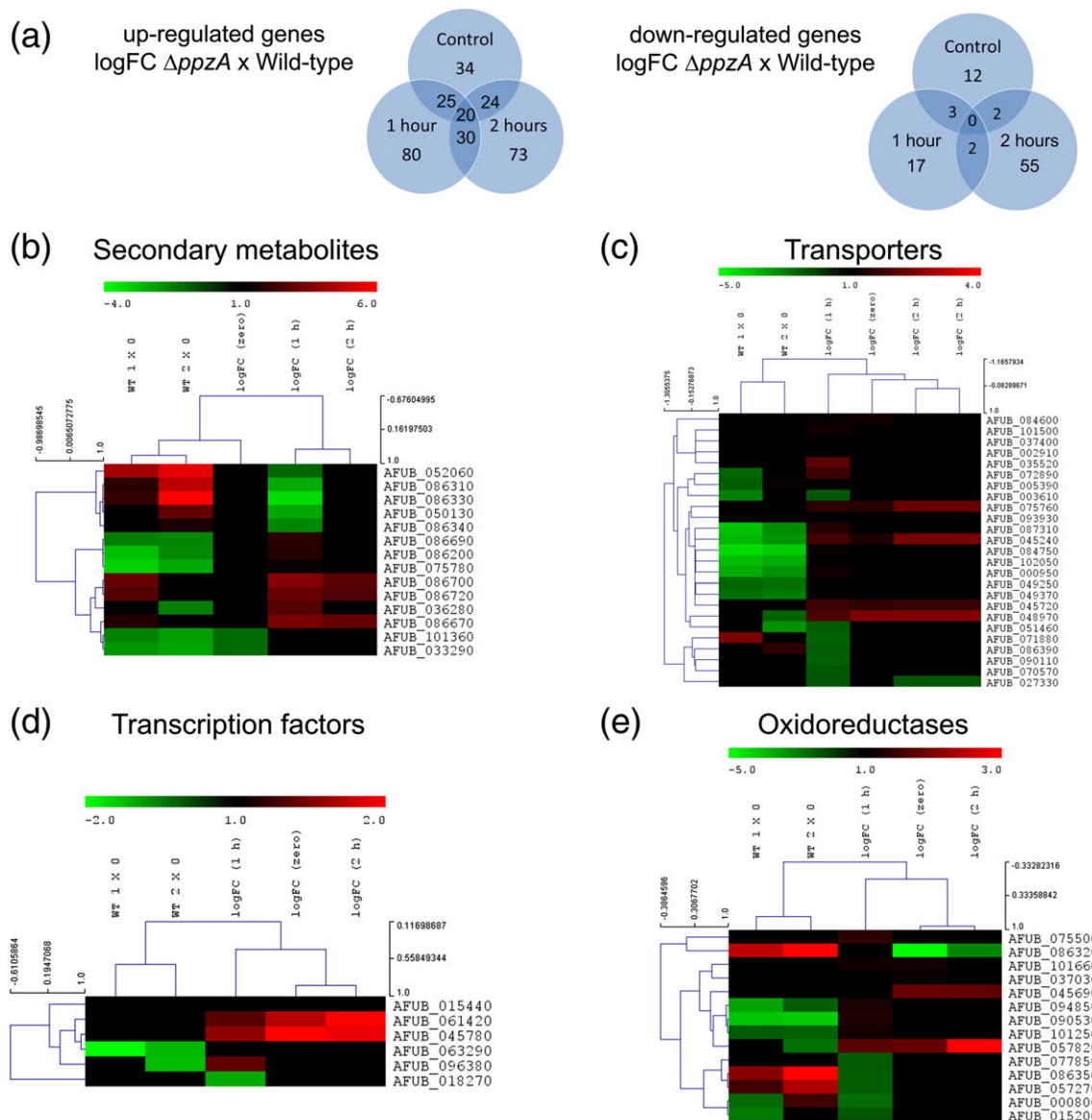| GO term	Description	p value	FDR	Class	Reg
GO:0006139	Nucleobase, nucleoside, nucleotide and nucleic acid metabolic process	2,53E-20	4,30E-18	BP	Up
GO:0006360	Transcription from RNA polymerase I promoter	0,000258	0,007101	BP	Up
GO:0033214	Iron assimilation by chelation and transport	0,002047	0,037272	BP	Up
GO:0032259	Methylation	0,000969	0,021466	BP	Up
GO:0016070	RNA metabolic process	2,35E-32	5,33E-30	BP	Up
GO:0090304	Nucleic acid metabolic process	9,10E-24	1,69E-21	BP	Up
GO:0006351	Transcription, DNA-dependent	0,0005	0,011894	BP	Up
GO:0015688	Iron chelate transport	0,002047	0,037272	BP	Up
GO:0042254	Ribosome biogenesis	3,55E-39	2,23E-36	BP	Up
GO:0009098	Leucine biosynthetic process	0,002047	0,037272	BP	Up
GO:0033212	Iron assimilation	0,002047	0,037272	BP	Up
GO:0070925	Organelle assembly	0,001745	0,034522	BP	Up
GO:0015891	Siderophore transport	0,002047	0,037272	BP	Up
GO:0006807	Nitrogen compound metabolic process	4,30E-15	4,87E-13	BP	Up
GO:0042375	Quinone cofactor metabolic process	4,73E-05	0,002143	BP	Down
GO:0006111	Regulation of gluconeogenesis	0,00279	0,046992	BP	Down
GO:0006970	Response to osmotic stress	0,002373	0,042009	BP	Down
GO:0055114	Oxidation–reduction process	0,000419	0,011197	BP	Down
GO:0072593	Reactive oxygen species metabolic process	0,000581	0,014987	BP	Down
GO:0019752	Carboxylic acid metabolic process	0,001581	0,032215	BP	Down
GO:0009408	Response to heat	0,000832	0,019958	BP	Down
GO:0006783	Heme biosynthetic process	0,002048	0,036938	BP	Down
GO:0042542	Response to hydrogen peroxide	0,000595	0,015145	BP	Down
GO:0051188	Cofactor biosynthetic process	6,55E-05	0,00278	BP	Down
GO:0009060	Aerobic respiration	0,000657	0,016122	BP	Down
GO:0045733	Acetate catabolic process	0,001148	0,025702	BP	Down
GO:0042168	Heme metabolic process	0,002048	0,036938	BP	Down
GO:0042180	Cellular ketone metabolic process	0,000263	0,008122	BP	Down
GO:0006082	Organic acid metabolic process	0,001581	0,032215	BP	Down
GO:0006066	Alcohol metabolic process	0,000394	0,010863	BP	Down
GO:0006091	Generation of precursor metabolites and energy	2,39E-06	0,000161	BP	Down
GO:0006083	Acetate metabolic process	0,000106	0,004153	BP	Down
GO:0006123	Mitochondrial electron transport, cytochrome c to oxygen	0,000271	0,008246	BP	Down
GO:0005975	Carbohydrate metabolic process	2,49E-08	3,62E-06	BP	Down
GO:0009628	Response to abiotic stimulus	0,001011	0,023421	BP	Down

Note. For the full list, refer to Table S1.

efflux transporter GliA (AFUB_075760/Afu6g09710), MFS alpha-glucoside transporter (AFUB_048970/ Afu5g00500), MFS sugar transporter (AFUB_084600/Afu8g02010), MFS quinate transporter (AFUB_072890/Afu6g06960), MFS myo-inositol transporter (AFUB_102050 Afu4g01560), sulphate transporter (AFUB_005390/Afu1g05020), and a putative siderochrome-iron transporter (AFUB_035520/Afu3g13670). Additionally, a downregulation of the low affinity iron transporter (AFUB_071880/Afu4g14640) was also observed. Although the PpzA phosphatase seems to be involved in iron assimilation, we did not identify differences in the expression of genes related to RIA and siderophore-mediated iron uptake (Tables S3 and S4). Interestingly, there was a downregulation of the protein phosphatase ptcG, which was also previously identified as a phosphatase involved in iron metabolism (Table S4; Winkelströter et al., 2015).

Some important genes involved in biosynthetic processes of SMs were also found to be differentially regulated. Among them, four genes belong the neosartoricin/fumicycline cluster, a cytochrome P450 monooxygenase, encoded in the putative gliotoxin biosynthetic gene cluster, and a PKS, encoded in the fma (fumagillin) SM gene cluster were upregulated in the ppzA mutant. Furthermore, genes encoding an enzyme involved in the biosynthesis of fumitremorgins and the PKS PksP were downregulated in the ppzA strain (Table S3). Therefore, this analysis of the transcriptome implies that PpzA has a broad influence on genes involved in secondary metabolism.

Previously, we have observed reduced mRNA accumulation of sidA and hapX in the ΔppzA mutant when compared to the wild-type strain by using RT-qPCR experiments (Winkelströter et al., 2015). We have used as normalizer for this set of qRT-PCR experiments
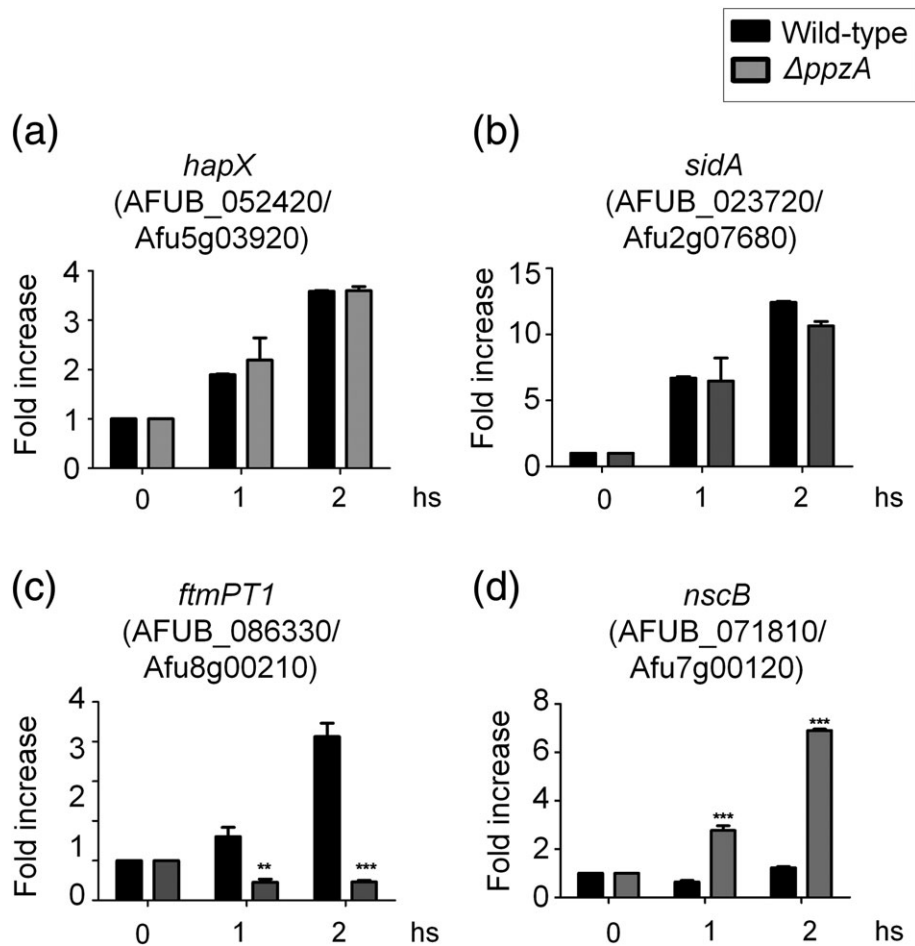
(a)

up-regulated genes
logFC ΔppzA x Wild-type

down-regulated genes
logFC ΔppzA x Wild-type

(b) Secondary metabolites

(c) Transporters

(d) Transcription factors

(e) Oxidoreductases

FIGURE 2 RNA seq data analysis of genes differentially regulated comparing ppzA to the wild-type strains under iron starvation. (a) Numbers of genes at least twofold differentially regulated comparing the ppzA to wild type (WT) under control and after iron starvation are represented in Venn diagrams. Numbers in overlapping areas represent common group of genes in the indicated comparison. ((b)–(e)) Heat map showing the enrichment analysis of the differentially expressed genes in some biological categories such as transcription factors, secondary metabolites, transporters, and oxidoreductases, in five comparisons. Column 1, WT 1 × 0 (1 hr of iron starvation/control); Column 2, WT 2 × 0 (2 hr of iron starvation/control); Column 3, ppzA/WT (control); Column 4, ppzA/WT (1 hr of iron starvation); and Column 5, ppzA/WT (2 hr of iron starvation). The colour scale represents the average expression ratios on a LogFC. Abbreviations: WT 1 × 0 fold change between wild type 1 hr of iron starvation and wild-type control; WT 2 × 0 fold change between wild type 2 hr of iron starvation and wild-type control; log FC (zero) fold change between ppzA and wild type under control; log FC (1 hr) fold change between ppzA and wild type after 1 hr of starvation; log FC (2 hr) fold change between ppzA and wild type after 2 hr of starvation

AFUB_010330/Afu1g10910 encoding the beta-tubulin. Here, FPKM analysis showed that, during our RNAseq experiments, there is a coefficient of variation of about 13% for this gene (data not shown). Accordingly, we decided to validate that sidA and hapX were transcriptionally induced in the wild-type and ΔppzA strains during iron starvation using RT-qPCR and independent RNA preparations (Figure 3a,b). However, in these experiments, AFUB_002930/Afu1g02550 (encoding a tubulin alpha-1 subunit) was used as normalizer because this gene was consistently expressed in both strains throughout our RNA-seq investigations of iron starvation (and it has much lower coefficient of variation, 4.59, than AFUB_010330, Afu1g10910). qRT-PCR experiments confirmed the expression levels observed for hapX

and sidA in the RNAseq experiments, that is, there are no significant differences in the hapX and sidA mRNA accumulation levels in the wild-type and ΔppzA mutant strains (Figure 3a,b). Aiming further validation of the RNAseq experiments, we also chose two genes, AFUB_086330/Afu8g00210 (ftmPT1 encoding a putative brevianamide F prenyltransferase predicted to convert brevianamide F to tryprostatin B; involved in the biosynthesis of fumitremorgins) and AFUB_086670/Afu7g00120 (nscB encoding a putative metallo-β-lactamase-like thioesterase that plays a role in neosartoricin A and fumicycline A biosynthesis) important for secondary metabolism (Figure 3c,d; König et al., 2013). The expression of these genes showed a high level of correlation with the RNA-seq data (Table S5).

FIGURE 3 The expression of (a) *hapX*, (b) *sidA*, (c) *ftmPT1*, and (d) *nscB*, as determined by qRT-PCR during iron starvation. The wild-type and Δ*ppzA* mutant strains were grown for 16 hr at 37 °C and transferred to iron starvation conditions for 1 and 2 hr, respectively. All gene expressions were normalised by the amount of AFUB_002930/Afu1g02550 (encoding a tubulin alpha-1 subunit). Standard deviations present the average of three independent biological repetitions (each with two technical repetitions). Statistical analysis was performed using a one-way analysis of variance test with post hoc test Dunnett when compared to the control condition (*p < .05)

Secondary metabolite gene clusters are enriched on rapidly evolving subtelomeric chromosomal regions (McDonagh et al., 2008), and their expression is influenced by both cluster-specific transcriptional activators and global chromatin factors. We therefore examined expression patterns across chromosome domains for evidence of general changes in chromatin structure in Δ*ppzA*. Mean expression across subtelomeric regions was significantly higher in Δ*ppzA* under iron replete conditions and remained higher during iron starvation. In contrast, expression from subcentromeric genes was activated under iron replete conditions but sharply reduced under iron starvation (Figure S2). Overall, the assignment of expression pattern to chromosome domain was significant by analysis of variance in a linear model fitting relative expression to additive and interaction effects of chromosome, chromosomal domain, and time under iron starvation (F = 20.5, p < 1 × 10^{-8} for domain, F = 2.8, p < 1 × 10^{-5} for domain:time:chromosome interaction). We also observed a change in correlation between mean expression from chromosomes (excluding centromeric and telomeric sequence) and their physical size, which increased with iron starvation. Although a trend toward lower expression from small chromosomes was present in both wild type and Δ*ppzA*, relative expression in Δ*ppzA* was highly negatively correlated with chromosome size (Pearson's r = −0.70, −0.75, and −0.96 at Time 0-, 1-,

and 2-hr iron starvation, respectively (Figure S3). The transcriptomic data and analysis of chromosomal patterns of gene expression in *ppzA* deletion mutant point toward involvement of PpzA in production of SM.

2.2 | Identification of putative PpzA target proteins by proteome analysis

We also used proteomics (spectral counts) to investigate proteins differentially abundant in the Δ*ppzA* mutant under iron starvation. A comparison of differentially abundant proteins showed that 133 and 36 were upregulated and downregulated in the *ppzA* strain after 2 hr of iron starvation, respectively (Tables S6 and S7). After 4 hr of starvation, 99 and 46 proteins were increased and decreased, respectively, in the *ppzA* strain compared to the wild type (Tables S6 and S7). A common group of 42 and 8 genes upregulated and downregulated, respectively, was identified between the two comparisons (Tables S6 and S7). Upon iron starvation, in Δ*ppzA*, there was an abundance reduction of proteins related to protein synthesis, DNA metabolism, and histones (Table 2). Some of the reduced abundance proteins identified are involved in oxidative, heat stress, and hypoxia, for example, the carbonic anhydrase Nce103 and AIF-like mitochondrial oxidoreductase

TABLE 2 Proteins identified as differentially expressed in the ΔppzA mutant strain upon growth on MM medium (control) and transfer to iron starvation (for 2 or 4 hr)

Functional category				
Feature ID	Description	LogFC ppzA/WT (zero)	LogFC ppzA/WT (2-hr iron starvation)	LogFC ppzA/WT (4-hr iron starvation)
Ergosterol biosynthesis				
AFUA_8G07210	Hydroxymethylglutaryl-CoA synthase, SrbA-regulated during hypoxia	−2,47062	ND	ND
Oxidative, heat stress, and hypoxia				
AFUA_2G05060	Alternative oxidase AlxA, transcriptionally induced in response to oxidative stress	ND	2,52324	2,35687
AFUA_3G14540	Heat shock protein Hsp30/Hsp42	−2,41293	−1,93296	−1,5649
AFUA_4G11250	Carbonic anhydrase Nce103	−2,25502	ND	ND
AFUA_7G02070	AIF-like mitochondrial oxidoreductase (Nfrl)	−2,06423	ND	−1,3924
AFUA_4G03410	Putative flavohemoprotein; protein induced by heat shock and hypoxia	−1,41991	ND	ND
AFUA_1G09890	Protein with Yap1-dependent induction in response to hydrogen peroxide	−1,28595	ND	ND
AFUA_5G12840	Hydroxyacylglutathione hydrolase, putative	−1,23838	ND	ND
AFUA_5G07320	Poly(ADP)-ribose polymerase PARP	−1,36653	ND	−1,1862
AFUA_5G02230	Putative actin interacting protein; protein induced by hydrogen peroxide	1,02422	ND	ND
AFUA_6G08360	Thiazole biosynthesis enzyme; hypoxia induced protein; induced by gliotoxin exposure	1,20362	ND	ND
AFUA_4G09090	Ortholog(s) have role in cellular response to alkyl hydroperoxide	1,2208	2,28807	2,80723
AFUA_5G06240	Putative zinc-dependent alcohol dehydrogenase	−1,93585	ND	ND
Protein synthesis				
AFUA_3G06760	60S ribosomal protein L37.	−1,00032	ND	ND
AFUA_2G02150	40S ribosomal protein S10a	−1,03277	ND	ND
AFUA_2G07970	60S ribosomal protein L19;	−1,15892	ND	ND
AFUA_1G16523	40S ribosomal protein S25	−1,37482	ND	ND
AFUA_2G10090	40S ribosomal protein S15	−1,46656	ND	ND
AFUA_6G13550	Ribosomal protein S13p/S18e	−1,19819	ND	ND
AFUA_3G10730	40S ribosomal protein S7e	−1,18402	2,32434	1,16157
AFUA_1G17120	Translation elongation factor eEF-1B gamma subunit, putative.	−1,51922	ND	ND
AFUA_5G06770	Ortholog(s) have role in cytoplasmic translation and cell tip, cytoplasm localisation	1,65628	ND	−1,14354
AFUA_6G04520	Ortholog(s) have protein-lysine N-methyltransferase activity	1,55291	ND	ND
Lipid metabolism				
AFUA_4G04410	Immunoreactive protein; has predicted 3-hydroxyacyl-CoA dehydrogenase activity	1,18877	−1,10303	ND
AFUA_3G04170	Ortholog(s) have pyruvate dehydrogenase activity and role in acetyl-CoA biosynthetic process from pyruvate, arginine biosynthetic process, glutamine biosynthetic process	1,11366	ND	ND
AFUA_1G14850	Putative acyl-CoA dehydrogenase with a predicted role in beta oxidation of fatty acids	1,2173	ND	ND
AFUA_7G05920	Stearic acid desaturase (SdeA)	−1,44084	ND	ND
AFUA_3G10750	Acetate kinase; calcium downregulated; SrbA-regulated during hypoxia	−1,58451	ND	ND
AFUA_5G08930	Putative isovaleryl-CoA dehydrogenase; ortholog of A. nidulans ivdA	2,65309	ND	ND
DNA metabolism and histones				
AFUA_5G02520	Ortholog(s) have DNA helicase activity, DNA replication origin binding,	−1,11046	ND	ND

(Continues)

TABLE 2 (Continued)

Functional category				
Feature ID	Description	LogFC *ppzA*/WT (zero)	LogFC *ppzA*/WT (2-hr iron starvation)	LogFC *ppzA*/WT (4-hr iron starvation)
	chromatin binding, single-stranded DNA binding activity			
AFUA_5G01940	Has domain(s) with predicted nucleic acid binding, nucleotide binding activity	−1,08757	ND	ND
AFUA_1G04900	Proliferating cell nuclear antigen (PCNA); conidia-enriched protein	1,18811	ND	−1,81784
AFUA_1G13790	Histone H3	−1,25674	ND	ND
AFUA_3G06070	Histone H1	−1,14675	ND	ND
AFUA_3G11030	Ortholog(s) have histone binding activity	1,44261	3,46336	2,21415
AFUA_2G02120	Ortholog(s) have phosphopentomutase activity, role in deoxyribose phosphate catabolic process and cytosol, nucleus localisation	−1,06546	ND	ND
AFUA_3G10920	Telomere and ribosome associated protein Stm1, putative	−1,05359	ND	ND
Secondary metabolism and siderophore biosynthetic pathway				
AFUA_5G12730	Putative nonribosomal peptide synthetase (NRPS) (Cluster 23)	1,28881	ND	ND
AFUA_3G03400	SidF	2,42004	ND	ND
AFUA_1G04450	SidL	ND	1,26242	ND
AFUA_8G00410	metAP, methionine aminopeptidase type II; encoded in the fma (fumagillin) secondary metabolite gene cluster (Cluster 33)	−1,53802	−1,17138	ND
AFUA_8G00370	Polyketide synthase, encoded in the fma (fumagillin) secondary metabolite gene cluster; required for fumagillin biosynthesis (Cluster33)	ND	ND	−1,97291
AFUA_8G00390	O-methyltransferase, putative, encoded in the fma (fumagillin) secondary metabolite gene cluster (Cluster 33)	ND	ND	−1,50156
AFUA_8G00510	Predicted oxidoreductase; encoded in the fma (fumagillin) secondary metabolite gene cluster (Cluster 33)	ND	ND	−1,29517
AFUA_8G00430	Ortholog of *A. nidulans* AN1088; hypoxia induced protein; encoded in the fma (fumagillin) secondary metabolite gene cluster (Cluster 33)	ND	ND	−1,14764
Afu1g17200	SidC	ND	ND	−1,12493
AFUA_1G17740	Hybrid NRPS/PKS enzyme (Cluster 4)	ND	ND	−1,09285
Afu8g00530	Putative alpha/beta hydrolase; member of the pseurotin A gene cluster (Cluster 34)	ND	ND	−1,07814
Afu6g09740	Thioredoxin reductase GliT (Cluster 26)	ND	ND	1,2237
Afu3g03640	MirB	ND	ND	1,5776
Transcription factor				
AFUA_5G08990	Transcription factor RfeG/ORF, uncharacterized	−1,13291	ND	ND
Miscellaneous				
AFUA_2G10030	Immunoreactive protein; calcium induced; transcript induced by exposure to human airway epithelial cells; induced by gliotoxin exposure	−1,12556	ND	ND
AFUA_1G07230	Has domain(s) with predicted protein disulfide oxidoreductase activity	−1,12468	ND	ND
AFUA_5G00130	Capsule polysaccharide biosynthesis protein, putative	−1,06591	ND	ND
AFUA_3G06720	ThiJ/PfpI family protein	−2,02283	ND	−1,11822
AFUA_4G01580	Putative uncharacterized protein	−1,91234	ND	ND
AFUA_8G05610	Cell wall glucanase (Scw11)—BtgE	−1,88953	ND	ND
AFUA_3G13110	Putative adhesin; extracellular serine−threonine rich protein	−1,85343	ND	ND

(Continues)

TABLE 2 (Continued)

Functional category				
Feature ID	Description	LogFC *ppzA*/WT (zero)	LogFC *ppzA*/WT (2-hr iron starvation)	LogFC *ppzA*/WT (4-hr iron starvation)
AFUA_6G13830	Oxidoreductase, short chain dehydrogenase/reductase family	−1,67885	ND	ND
AFUA_3G03060	Cell wall protein PhiA	−1,62568	ND	−1,57815
AFUA_6G13490	Glutamate decarboxylase	−1,61013	ND	ND
AFUA_2G11120	Has domain(s) with predicted methyltransferase activity	−1,54461	ND	ND
AFUA_4G00390	Glycosyl hydrolase, putative	−1,45462	ND	ND
AFUA_4G03490	Tripeptidyl-peptidase (TppA)	−1,51889	ND	ND
AFUA_1G14170	Beta-galactosidase	−1,30075	−1,09472	−1,11773
AFUA_3G07680	Putative ran GTPase activating protein	2,48007	2,10589	3,987
AFUA_1G06370	Ortholog(s) have role in meiotic nuclear division and cytosol, nucleus localisation	1,68424	ND	4,56409
AFUA_6G05340	Ortholog(s) have tryptophan-tRNA ligase activity, role in mitochondrial tryptophanyl-tRNA aminoacylation and mitochondrion localisation	2,27365	ND	ND
AFUA_5G08170	Ortholog(s) have Atg8 ligase activity and role in C-terminal protein lipidation	1,10566	1,67075	ND
AFUA_4G02790	Has domain(s) with predicted hydrolase activity	1,12296	ND	ND
AFUA_6G12170	Putative FK506-binding protein (FKBP)-type peptidyl-prolyl cis-trans isomerase	−1,00988	1,74046	ND
AFUA_4G12100	Ortholog(s) have role in cellular response to biotic stimulus, cellular response to starvation and cytoplasmic translation	1,37361	ND	ND
AFUA_3G11350	ATPase; proteins are recognised and bound by Get3p then delivered to the ER	1,18883	ND	ND
AFUA_2G12900	Ortholog(s) have urease activity, role in urea catabolic process	1,21037	ND	ND
AFUA_2G13630	Putative amino transferase; immunoreactive	1,45445	ND	ND
Unknown function				
AFUA_3G00960	Putative uncharacterized protein	−1,26313	ND	ND
AFUA_2G10170	Putative uncharacterized protein	−1,22204	ND	ND
AFUA_3G00350	Putative uncharacterized protein	−1,1774	ND	ND
AFUA_2G09140	Putative uncharacterized protein	−1,14675	ND	ND
AFUA_1G00760	Putative uncharacterized protein	−1,06135	ND	ND
AFUA_2G15290	Conidia-enriched protein of unknown function; transcript downregulated in response to voriconazole; hypoxia repressed protein	−2,34076	2,38262	2,60457
AFUA_1G04680	Ortholog(s) have mitochondrion localisation	1,57479	ND	1,15881
AFUA_4G14060	Has domain(s) with predicted ATP binding activity	1,5816	ND	ND
AFUA_6G10450	Hypothetical protein	1,11263	ND	ND
AFUA_5G12780	Kelch repeat protein	−1,26703	−1,24122	ND
AFUA_3G14280	Ortholog(s) have cytosol localisation	2,37552	ND	3,97775
AFUA_1G10960	Ortholog(s) have cytosol, nucleus localisation	1,09224	ND	ND
AFUA_1G03180	Has domain(s) with predicted carbon-sulphur lyase activity and role in metabolic process	2,31507	2,38262	2,60457

Note. For the full list, refer to Table S3. ND = no difference.

(Nfrl). In Δ*ppzA*, there was an increase of the SidL and SidF siderophore biosynthetic machinery components and MirB, a siderophore iron transporter. Conversely, there was a reduction of SidC, an NRPS involved in ferricrocin siderophore biosynthesis, in Δ*ppzA*, after 4 hr of starvation. The alternative oxidase protein (AoxA), which is transcriptionally induced in response to oxidative stress, was increased in abundance in Δ*ppzA* under iron starvation. Moreover, there was a reduction of some proteins involved in fumagillin and pseurotin A biosynthetic processes and an increase of GliT, a gliotoxin oxidoreductase required for gliotoxin biosynthesis. Therefore, this proteomic analysis suggests the involvement of PpzA in regulation of siderophore biosynthesis and SM production.

Finally, comparison of RNAseq and proteomics data shows few (11) targets modulated at the two levels (Afu2g17500/AFUB_084820, Afu8g00370/AFUB_018370, Afu1g17200/AFUB_016590, Afu3g03400/AFUB_044850, Afu5g01690/AFUB_050220, Afu2g02630/AFUB_019730, Afu1g02820/AFUB_003200, Afu1g17250/AFUB_057130, Afu1g04450/AFUB_004790, Afu3g14940/AFUB_034300, and Afu2g00500/AFUB_017560). From these, three (Afu1g17200, Afu3g03400, and Afu1g04450) were only differentially regulated in the RNAseq experiments in both the wild-type and Δ*ppzA* mutant strains upon iron starvation. These genes encode *sidC*, *sidL*, and *sidF*, respectively, important for siderophore biosynthesis. In contrast, two genes with unknown functions (Afu5g01690 and Afu2g02630) were only differentially expressed in the RNAseq experiment in the Δ*ppzA* mutant but not in the wild-type strain. Finally, the remaining six genes were differentially expressed at both RNAseq and proteomics analyses, with orthologous with roles in cyanide catabolic process (Afu2g17500), fumagillin biosynthesis (Afu8g00370), NADH-quinone oxidoreductase (Afu1g02820), assembly of spore wall (Afu1g17250), enzyme inhibition activity (Afu3g14940), and unknown functions (Afu2g00500). Taken together, these data evidences the complex regulatory effects of PpzA in *A. fumigatus*.
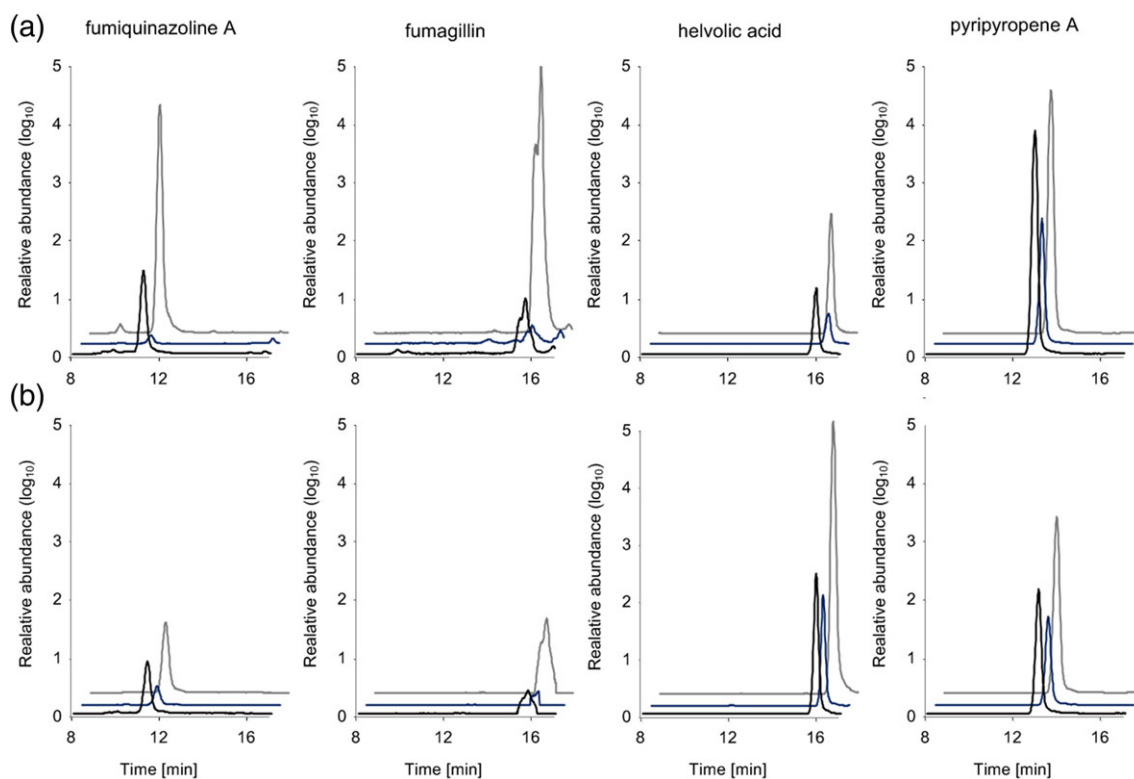
2.3 | PpzA phosphatase is important for SM biosynthesis

Aspergillus fumigatus yields a huge number of SMs that have several functions including their role as virulence factors (Berthier et al., 2013; Bok et al., 2006; Heinekamp et al., 2012; Jahn, Langfelder, Schneider, Schindel, & Brakhage, 2002; Macheleidt et al., 2016; Yin et al., 2013). Interestingly, transcriptome and proteome analysis demonstrated that diverse SM gene clusters showed altered expression in *ppzA*. The relative amount of several SMs produced in the *ppzA* mutant in comparison with the wild type was analysed by liquid chromatography–mass spectrometry (LC-MS) under standard and iron starvation conditions (Figure 4). The *ppzA* mutant clearly lacked SM production in both iron replete and iron starvation conditions. SM profiling in the presence of iron starvation showed that the Δ*ppzA* mutant had reduced production of fumiquinazoline A, fumagillin, helvolic acid, pyripyropene A (Figure 4a), and triacetyl-fusarinine C (data not shown). In iron repletion, Δ*ppzA* showed reduced levels of fumiquinazoline A, helvolic acid, and pyripyropene A (Figure 4b). Interestingly, the complementing strain has increased or comparable SM production than the wild-type strain (Figure 4). Taken together, these results clearly demonstrate that phosphatase PpzA plays a role in SM production in *A. fumigatus*.

2.4 | MpkA and SakA activation during iron starvation is not affected by PpzA

The MAP kinase MpkA controls iron adaptation in *A. fumigatus* and iron starvation activates MAPK through its phosphorylation (Jain et al., 2011). To evaluate if PpzA participate in the MpkA pathway in *A. fumigatus*, the phosphorylation state of the MpkA was determined during iron starvation. The phosphorylation levels of the MpkA protein were determined using the anti-p44/42 MAPK antibodies directed against phosphorylated MpkA. The wild-type and mutant strains were
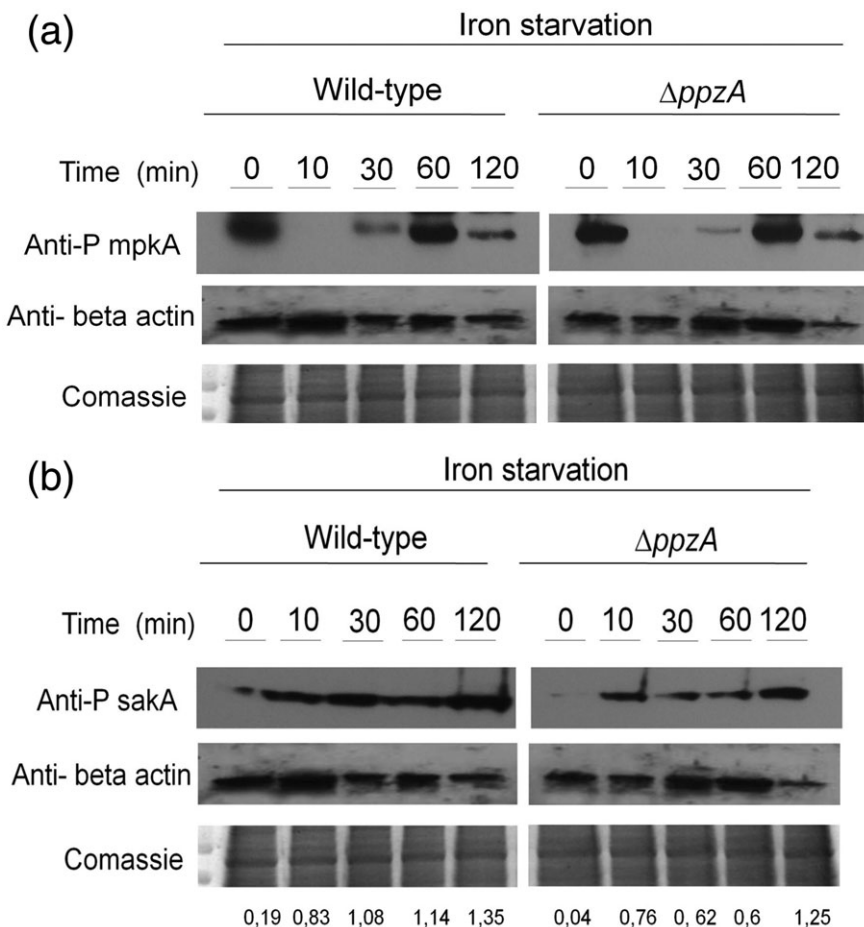

FIGURE 4 Production of secondary metabolites (SMs) in *A. fumigatus* wild-type (black), Δ*ppzA* (blue), and complemented (grey) mutant strains during (a) iron depletion and (b) iron repletion conditions. Depicting extracted ion chromatograms (EIC) of different metabolites for m/z 446.18 $[M + H]^+$ for fumiquinazoline A, m/z 459.23 $[M + H]^+$ for fumagillin, EIC m/z 567.29 $[M + H]^-$ for helvolic acid, and m/z 584.24 $[M + H]^+$ for pyripyropene A

grown in iron-sufficient MM overnight, and samples were collected before and after iron starvation conditions (10, 30, 60, and 120 min). In the wild-type strain, the phosphorylation of MpkA initially decreased and subsequently increased after 60 min demonstrating that iron starvation modulates MpkA phosphorylation. The ppzA strain had levels of MpkA phosphorylation similar to the wild type under iron depletion and iron repletion conditions (Figure 5a). In A. fumigatus, SakA is the most important stress-activated MAPK in hyphal growth (Hagiwara, Suzuki, Kamei, Gonoi, & Kawamoto, 2014). To determine if ΔppzA was involved in SakA response to iron starvation, the phosphorylation state of SakA was determined. The phosphorylation levels of the SakA protein were determined using the antiphospho-p38 MAPK (Thr180/Tyr182) antibody. In both the wild-type and ΔppzA strains, the SakA phosphorylation levels significantly increase during iron starvation (10, 30, 60, and 120 min). The SakA phosphorylation levels in the wild-type and ppzA mutant were similar in control and after iron starvation (Figure 5b). These results indicate that A. fumigatus MpkA and SakA are phosphorylated during iron starvation but this phosphorylation is not significantly affected by PpzA.

2.5 | Identification of proteins that interact with PpzA

The above results suggest that PpzA plays an important role in pathways that affect the iron-dependent secondary metabolism network. To identify PpzA-interacting proteins, we generated a strain in which the ppzA gene was replaced by an allele encoding a TAP-tag epitope fusion protein. This strain showed wild-type growth indicating the

functionality of the PpzA-TAP fusion protein (Figure S4). We performed protein pull-down experiments aiming to identify interaction partners of PpzA by mass spectrometry assays. Protein extracts were prepared from wild-type and PpzA::TAP-tag strains under iron-replete (control) and iron starvation conditions (2 and 4 hr). We have compared the proteins immunoprecitated with the PpzA::TAP-tag and wild-type strains and removed the proteins precipitated by the latter because they are potential artefacts (for proteins immunoprecipitated in the wild type, see Table S8). The full group of proteins that co-purified with PpzA before and after iron starvation are listed in Table 3 and Table S9. These results show that PpzA interacts with at least 54 proteins, of which 31 were detected only after iron starvation and 22 were detected only in control conditions. Only one of these proteins, the regulatory subunit of the protein phosphatase PP1 (Afu1g04800/AFUB_005140), was common to both groups, suggesting that PpzA interactions are very dynamic and do not last too long. Other proteins that co-purified with PpzA include some ribosomal proteins (Afu1g06770/AFUB_007150, Afu2g07380/AFUB_023440, Afu2g07970/AFUB_023990, Afu2g16880/AFUB_032560, Afu4g07730/AFUB_064830, and Afu7g02140/AFUB_088700) and two pyruvate dehydrogenase complex components. The Afu3g14540/AFUB_034690 and Afu6g06470/AFUB_034690 are two putative heat shock proteins also identified in the PpzA interactome. Although MpkA phosphorylation was not significantly affected in the ΔppzA mutant, MpkA was identified as an interaction partner of PpzA only after 2 hr of iron starvation. Our results show that PpzA interacts physically with proteins that participate in different types of

FIGURE 5 MpkA and SakA phosphorylation during iron starvation are not affected by PpzA. Western blot analysis for the A. fumigatus phosphorylated MpkA (a) and SakA (B). The wild-type and ΔppzA strains were grown for 24 hr at 37 °C and transferred to MM without iron plus 200 μM BPS and 300 μM ferrozine for 10, 30, 60, and 120 min. Antibody against β actin was used as loading control

TABLE 3 Proteins that interact with ppzA upon growth on MM medium (control) and transfer to iron starvation (for 2 or 4 hr)

Functional category					
Accession	Description	Control	Iron starvation (h)	Iron starvation (h)	MW [kDa]
Cell cycle/signal transduction					
Afu1g04800	Ortholog(s) have protein phosphatase type 1 activator activity, role in positive regulation of mitotic sister chromatid separation, regulation of mitotic metaphase/anaphase transition and cytosol, nucleus localisation	0	2	4	39,3
Afu2g05740	Putative Rho-type GTPase	0	NI	NI	21,4
Afu4g08820	Predicted GDP/GTP exchange factor for G proteins, required for conidiation; partially complements A. nidulans ricA mutation (ricA)		2	NI	51,7
Afu4g13720	Mitogen-activated protein kinase; activated by phosphorylation; role in cell wall signalling and the oxidative stress response; mpkA(p)-lacZ expression increased by cell wall disturbing compounds; required for adaptation to iron starvation (mpkA)	NI	2	NI	48,4
Afu6g06900	Putative Rho-type GTPase; predominantly localise to the hyphal tip; involved in radial growth and conidiation; mutants display cytoplasmic leakage at the hyphal tips (rho1)	NI	2	NI	21,7
Afu6g13300	GTP-binding nuclear protein Ran	NI	NI	4	24,1
Histone/DNA damage response					
Afu1g13790	hhtA histone H3	0	NI	NI	15,3
Protein biosynthesis					
Afu1g06770	40S ribosomal protein S26	0	NI	NI	13,46017974
Afu2g07380	Ribosomal protein L18	0	NI	NI	20,8
Afu2g07970	60S ribosomal protein L19	0	NI	NI	22,6
Afu2g16880	60S ribosomal protein L37a	0	NI	NI	10,14944834
Afu4g07730	60S ribosomal protein L11; transcript induced by exposure to human air way epithelial cells	NI	2	NI	20,10062129
Afu7g02140	40S ribosomal protein S24	NI	NI	4	15,30539977
Afu1g03970	Putative mitochondrial translation initiation factor IF-2	0	NI	NI	118,6
Afu1g05200	tif32 eukaryotic translation initiation factor 3 subunit A	0	NI	NI	120,2
Afu4g03860	nip1 eukaryotic translation initiation factor 3 subunit C	NI	2	NI	97,44806195
Energy metabolism/ mitochondrial function					
Afu1g06960	Putative pyruvate dehydrogenase complex subunit alpha; protein induced by hydrogen peroxide; hypoxia induced protein	0	NI	NI	41,5
Afu7g05720	Pyruvate dehydrogenase complex, dihydrolipoamide acetyltransferase component; hypoxia induced protein	NI	NI	4	51,99925296
Fatty acid metabolism					
Afu3g12120	ppoC putative fatty acid oxygenase	NI	2	NI	126,3811646
Afu3g13970	Ortholog(s) have phosphatidylserine decarboxylase activity		2		120
Oxidative, heat stress, and hypoxia					
Afu2g04700	Ortholog(s) have role in cellular response to heat and cytosol, endoplasmic reticulum, nuclear outer membrane-endoplasmic reticulum membrane network localisation	0	NI	NI	142,3
Afu3g14540	hsp30 putative 30-kilodalton heat shock protein; conidia-enriched protein; protein levels increase in response to amphotericin B and hydrogen peroxide	NI	2	NI	20,5
Afu4g11340	lys9 AspGDID:ASPL0000106843 COORDS: Chr4_A_fumigatus_Af293:2978580-2976809C,	NI	2	NI	49,4

(Continues)

TABLE 3 (Continued)

Accession	Description	Control	Iron starvation (h)	Iron starvation (h)	MW [kDa]
Functional category					
	translated using codon Table 1 (450 amino acids) uncharacterized ORF; Saccharopine dehydrogenase; hypoxia induced protein; transcript induced by exposure to human airway epithelial cells				
Afu6g02750	egd1 nascent polypeptide-associated complex (NAC) subunit beta; protein level decreases upon heat shock	NI	2	NI	20,5
Afu6g06470	Putative integral plasma membrane heat shock protein; transcript downregulated in response to amphotericin B and to to voriconazole; induction in response to hydrogen peroxide Yap1-dependent	NI	2	NI	21,61985947
Transcription from RNA polymerase II promoter					
Afu3g11390	Ortholog(s) have role in positive regulation of RNA polymerase II transcriptional preinitiation complex assembly, proteasome regulatory particle assembly, ubiquitin-dependent protein catabolic process	NI	2	NI	51,56765165
Miscellaneous					
Afu2g09310	Has domain(s) with predicted proton-transporting ATP synthase activity, rotational mechanism, proton-transporting ATPase activity, rotational mechanism activity and role in ATP synthesis coupled proton transport	0	NI	NI	7,857137865
Afu2g12900	Ortholog(s) have urease activity, role in urea catabolic process and cytosol, nucleus localisation	0	NI	NI	29,1577844
Afu3g05360	Has domain(s) with predicted DNA binding, protein heterodimerization activity, role in nucleosome assembly and nucleosome, nucleus localisation	0	NI	NI	29,78166069
Afu3g06880	snxA sorting nexin	0	NI	NI	16,74452311
Afu3g10100	Ortholog(s) have role in mRNA export from nucleus and nucleus localisation	0	NI	NI	35,1
Afu3g11260	Ubiquitin	0	NI	NI	17,66146574
Afu6g06780	rpt4 AspGDID:ASPL0000109040 COORDS: Chr6_A_fumigatus_Af293:1481801-1483206 W, translated using codon Table 1 (393 amino acids) uncharacterized ORF;]proteasome regulatory particle subunit; transcript induced by exposure to human airway epithelial cells	0	NI	NI	44,08525382
Afu3g12900	hasB putative transporter; absolutely required for hexadehydroastechrome biosynthesis; orthologous member of the "has" secondary metabolite biosynthetic gene cluster of strain A1163	NI	2	NI	47,8
Afu4g04660	Afu4g04660 Ortholog(s) have protein domain specific binding activity	NI	2	NI	43,42297153
Afu4g10350	ubiD AspGDID:ASPL0000106749 COORDS: Chr4_A_fumigatus_Af293:2705133-2706130 W, translated using codon Table 1 (314 amino acids) uncharacterized ORF; Polyubiquitin; calcium induced	NI	2	NI	35,17775607
Afu5g02030	Has domain(s) with predicted mRNA binding activity, role in mRNA polyadenylation and mRNA cleavage factor complex localisation	NI	2	NI	37,6
Afu5g05570	Ortholog(s) have ATP binding, nucleoside-triphosphatase activity	NI	2	NI	20,2900565
Afu5g07050	Proteasome regulatory particle subunit; transcript induced by exposure to human airway epithelial cells	NI	2	NI	51,41750128
Afu5g11560	Ortholog(s) have ATP binding activity	NI	2	NI	47,62105126
Afu5g11720	Ortholog(s) have role in proteasome-mediated ubiquitin-dependent protein catabolic process and cytosol, nucleus localisation	NI	2	NI	100,7364685
Afu6g12400	fks1 putative 1,3-beta-glucan synthase catalytic subunit, major subunit of glucan synthase; predicted transmembrane protein; essential	NI	2	NI	218

(Continues)

TABLE 3 (Continued)

Functional category					
Accession	Description	Control	Iron starvation (h)	Iron starvation (h)	MW [kDa]
Afu6g13540	cp3 carboxypeptidase Y; predicted signal sequence for secretion; transcript up-regulated in conidia exposed to neutrophils; induced by growth on BSA as a sole nitrogen source	NI	NI	4	60,9
Afu7g04290	Putative amino acid permease; transcript up-regulated in conidia exposed to neutrophils and by growth on BSA as a sole nitrogen source	NI	NI	4	63,2
Afu8g04730	Oligopeptidase family protein	NI	NI	4	79,9
Unknown function					
Afu1g09130	Protein of unknown function identified by mass spectrometry	0	NI	NI	80,7
Afu1g15200	Ortholog of *A. nidulans* FGSC A4—AN3519, AN2646, AN0587, AN0866, and AN7370—and *A. fumigatus* Af293—Afu3g03790, Afu4g14040, Afu5g06900, and Afu7g08575	0	NI	NI	79,98259359
Afu3g10800	Ortholog of *A. nidulans* FGSC A4: AN4908; *A. niger* CBS 513.88: An02g06530; *A. oryzae* RIB40: AO090003000629; *A. wentii*: Aspwe1_0036953; and *Aspergillus sydowii*: Aspsy1_0043015	0	NI	NI	145,9
Afu4g08480	Afu4g08480 AspGDID:ASPL0000106562 COORDS: Chr4_A_fumigatus_Af293:2190795-2194480 W, translated using codon Table 1 (1140 amino acids) uncharacterized ORF; Ortholog(s) have cytosol, nucleus localisation	NI	2	NI	124,7
Afu4g14040	Ortholog of *A. nidulans* FGSC A4—AN3519, AN2646, AN0587, AN0866, and AN7370 and *A. fumigatus* Af293—Afu1g15200, Afu3g03790, Afu5g06900, and Afu7g08575	NI	2	NI	68,02350554
Afu5g07340	Ortholog(s) have cytosol, nucleus localisation	NI	2	NI	39,9
Afu7g03800	Ortholog of *A. nidulans* FGSC A4—AN4273; *A. niger* CBS 513.88—An13g00220; *A. oryzae* RIB40—AO090026000834; *Aspergillus wentii*—Aspwe1_0026252; and *Aspergillus sydowii*—Aspsy1_1088954	NI	NI	4	61,8

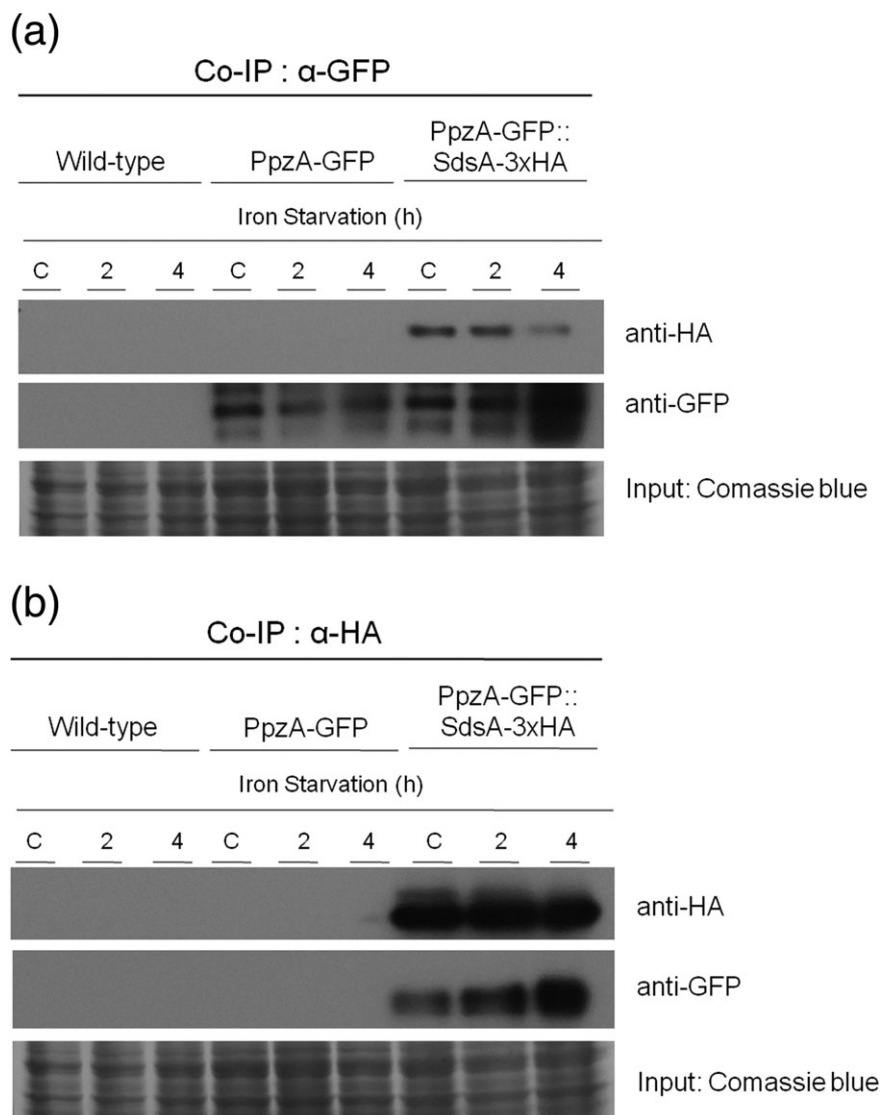*Note.* NI = No interaction, the protein was not identified in this time point.

stress response as in the regulation of the cell cycle, signal transduction, energy metabolism, and mitochondrial function.

To validate our strategy to identify PpzA-interacting proteins and confirm the biological importance of the observed PpzA interactions, we decided to investigate in more detail the interaction between PpzA and the protein encoded by Afu1g04800/AFUB_005140, here named SdsA because it is the putative *Saccharomyces cerevisiae* (*S. cerevisiae*) Sds22p homologue (*SDS22* encodes a regulatory subunit of PP1 Glc7p; Identity = 49.2%, similarity = 67.0%; e-value = 4e-73). With heterokaryon rescue assay and subsequent Southern blot analysis, we could show that *sdsA* is essential for *A. fumigatus* (Figure S5). We utilised a coimmunoprecipitation (Co-IP) approach introducing a 3xHA tag to the C-terminus of SdsA in the background of the green fluorescent protein (GFP)-tagged PpzA strains. We observed no changes in the phenotypes of these tagged strains compared to the wild type (Figures S6 and S7). We carried out Co-IP assays using GFP-Trap beads with the wild-type, GFP-tagged PpzA, and GFP-tagged PpzA and HA-tagged SdsA strain. The results of the immunoblotting analysis showed that SdsA coimmunoprecipitated from only the GFP-tagged PpzA and HA-tagged SdsA strain, corroborating the occurrence of PpzA–SdsA

interaction previously observed by pull-down experiments (Figure 6 a). To further confirm the specificity of this interaction, we performed reciprocal Co-IP assays using anti-HA antibodies coupled to magnetic beads. The results demonstrated that PpzA is co-immunoprecipitated with SdsA (Figure 6b). These results clearly demonstrate that PpzA and SdsA interact in *A. fumigatus*.

2.6 | PpzA is important for *A. fumigatus* virulence in a low-dose murine infection

The virulence of the Δ*ppzA* mutant strain was evaluated in a neutropenic murine model of invasive pulmonary aspergillosis. As shown in Figure 5a, immunocompromised animals infected with wild type resulted in 100% mortality after 12 days postinfection. In contrast, animals infected with Δ*ppzA* mutant showed a reduced mortality rate, to approximately 15%, after 15 days postinfection. The reconstituted strain was generated, and no significant difference was observed in the mortality rate of the animals infected with the wild-type and the complemented Δ*ppzA::ppzA*+ strain (Figure 7a).

FIGURE 6 PpzA interacts with SdsA. Validation of interaction between PpzA and SdsA identified by MS. Affinity purification assays from HA-tagged SdsA strains in the background of GFP-tagged PpzA were performed with (a) GFP-Trap beads and (b) anti-HA beads to verify interactions. The coimmunoprecipitated proteins were analysed by the antibodies indicated
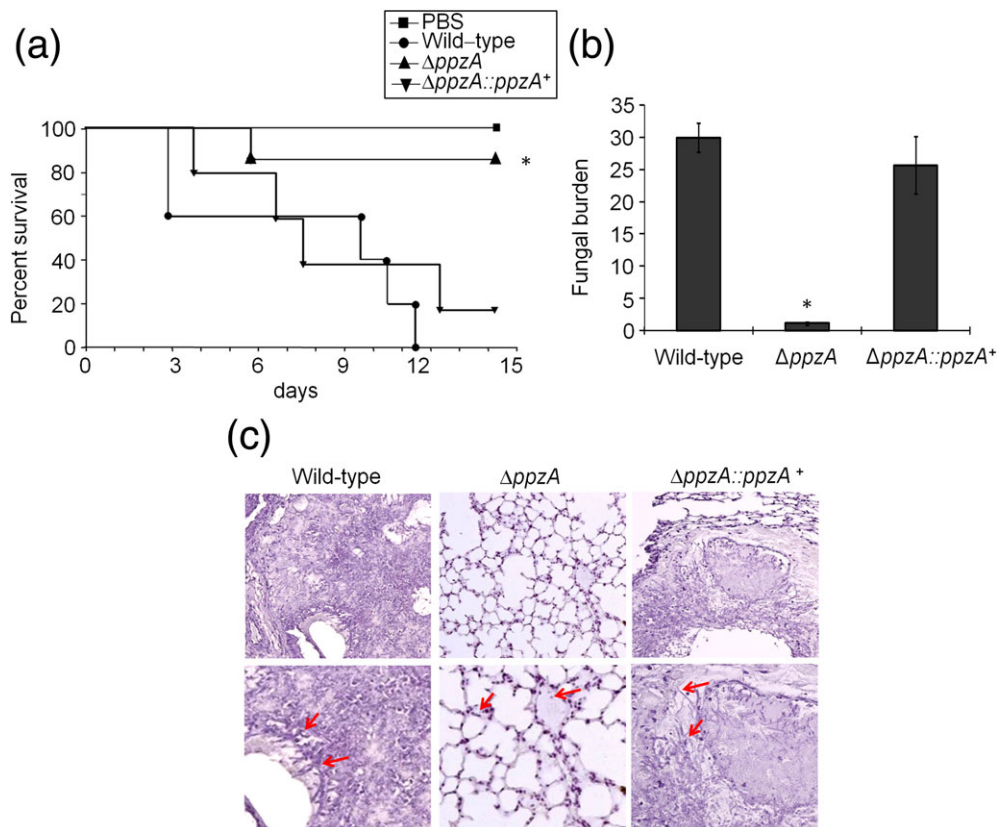
Fungal burden of the infected lung tissue was measured by qPCR. We found that Δ*ppzA* strain grows significantly less within the lungs when compared with the wild-type and the complemented strains (Figure 7b). Histopathological analysis shows multiple hyphae in the lungs of mice infected with the wild-type strain or reconstituted strain. In opposition, few hyphae were observed in the lungs of mice infected with Δ*ppzA* (Figure 7c). Taken together, these results indicate that PpzA plays an important role in *A. fumigatus* virulence.

3 | DISCUSSION

Micronutrient restriction imposed by mammalian hosts during an infection is a common mechanism of defence to reduce or avoid the pathogen infection. This mechanism has been known as nutritional immunity (Ganz, 2009). Iron is essential for survival of the organisms due to its involvement in several biological processes. Thus, iron availability during the infection process is related to a pathogen's ability to cause disease and to the host's ability to overcome infection. Much evidence shows that the frequency and the severity of infections

caused by different microorganisms, including fungi, bacteria, protozoa, and virus, increase with iron overload in humans (Drakesmith & Prentice, 2008; Khan, Fisher, & Khakoo, 2007). Facing an iron restriction condition imposed by hosts, pathogens such as fungi have developed high-affinity mechanisms to acquire this micronutrient, because it is fundamental for infection success (Cassat & Skaar, 2013). Iron uptake for *A. fumigatus* includes two high-affinity mechanisms: RIA and siderophore-assisted iron uptake (Hortschansky et al., 2007; Schrettl & Haas, 2011; Schrettl et al., 2004). Although the two main transcription factors involved in iron assimilation, SreA and HapX, have been well characterised (Schrettl et al., 2008; Schrettl et al., 2010), very little is known about the signal transduction pathways that regulate them. *A. fumigatus* MAP kinase MpkA, TOR (target of rapamycin), and SchA^SCH9 have been implicated in the control of amino acid and siderophore biosynthesis upon iron starvation (Valiante et al., 2009; Baldin et al., 2015; Alves de Castro et al., 2016).

Recently, we have characterised several *A. fumigatus* protein phosphatase null mutants that are associated to iron assimilation because they have reduced growth during iron starvation (Winkelströter et al., 2015). Among these protein phosphatases, we have identified the

FIGURE 7 PpzA is important for virulence in neutropenic mice. (a) Comparative analysis of mice infected with conidia from wild-type, *ppzA*, and complemented strains. Mice in groups of 10 per strain were infected intranasally with a 20 μl suspension of conidia at a dose of 10^5. (b) Quantification of fungal burden [fungal DNA(ng)/mouse DNA (ng)] was done 72 hr post infection by qPCR based on 18S rRNA gene of *A. fumigatus* and an intronic region of the mouse GAPDH gene. (c) Representative histological analyses of infection murine lung 72 hr post infection

gene *ppzA* that codes for the catalytic subunit of PPZ and it was previously shown to be involved in oxidative stress tolerance (Leiter et al., 2012; Muszkieta et al., 2014). Here, we investigated the role played by PpzA during iron assimilation by using a combined transcriptomic and proteomic analysis comparing the corresponding wild-type strain with *ppzA* mutant under iron starvation conditions. We show that *A. fumigatus* PpzA participates directly or indirectly in posttranslational alterations that influence the response to iron assimilation, affecting not only siderophore production but also the transcription of several genes involved in the biosynthesis of SMs. Our results revealed that PpzA regulates the expression of many genes involved in oxidation–reduction processes. However, our transcriptome analysis cannot explain why PpzA is necessary for adequate responses against oxidative stress. In addition, the proteomic analysis demonstrated that AoxA was increased in Δ*ppzA* under iron starvation. In *A. fumigatus*, AoxA activity and mRNA expression were both induced in presence of oxidative stress and the strain with *aoxA* deletion was more exposed to killing by macrophages (Magnani et al., 2008). However, the alternative oxidase is not necessary for *A. fumigatus* virulence in an immuno-suppressed murine model of infection (Grahl, Dinamarco, Willger, Goldman, & Cramer, 2012).

A notable result of the RNAseq analysis of *ppzA* was the detection of differential regulation of genes involved in biosynthesis of some SM gene clusters. It has been demonstrated that both SreA and HapX loss perturbed SM production (Wiemann et al., 2014). The production of

pseurotin A, fumagillin, and terezine D was significantly higher with increasing iron concentrations, suggesting that SreA should trigger activating effects during iron overload conditions (Wiemann et al., 2014). In support to this hypothesis, the induction of pseurotin A and fumagillin was lost in the Δ*sreA* mutant. HapX deficiency alters the production of SM mainly under iron-restricting conditions, where HapX appears to function as a repressor (Wiemann et al., 2014). SM gene cluster expression is governed by both global and cluster-specific transcriptional regulators, signal transduction pathways, and epigenetic regulation (Macheleidt et al., 2016). The G protein-coupled receptor signalling pathways have been reported as one of the main signal transduction mechanisms involved in the regulation of secondary metabolism in *Aspergilli* (Brodhagen & Keller, 2006; Gehrke, Heinekamp, Jacobsen, & Brakhage, 2010; Hicks, Yu, Keller, & Adams, 1997). Furthermore, MAP kinase pathways and adenylyl cyclase/cAMP/PKA pathways are downstream effectors of G protein-coupled receptors (Brodhagen & Keller, 2006; Grosse, Heinekamp, Kniemeyer, Gehrke, & Brakhage, 2008). There are few studies connecting phosphatases to the production of SM in fungi. One study in *Fusarium graminearum* that reported 11 phosphatase deletion mutants impaired in virulence also showed reduced biosynthesis of the mycotoxin deoxynivalenol (DON; Yun et al., 2015), an important virulence factor for this species (Ding et al., 2009).

The transcriptome data shown here demonstrated that many genes of neosartoricin/fumicycline cluster were upregulated in the

ppzA strain. This cluster is responsible for the production of an unusual prenylated polyphenol (fumicycline A) through the meroterpenoid pathway, which is regulated by epigenetic factors and a pathway-specific activator gene (König et al., 2013) Furthermore, the RNA-seq analysis here showed that the expression of the cytochrome P450 monooxygenase, a gene of the gliotoxin biosynthesis cluster, was increased in ppzA. Gliotoxin belongs to the epipolythiodioxopiperazine class of SM. These natural products present several biological activities, such as antiviral and antifungal properties, as well as exhibiting in vitro and in vivo immunomodulatory activity. Gliotoxin is an important factor for *A. fumigatus* virulence depending on the host immune status, but it can also inhibit fungal development, as *A. fumigatus* growth (Carberry et al., 2012; Chotirmall, Mirkovic, Lavelle, & McElvaney, 2014; Scharf et al., 2010). Previous results showed that *ppzA* deletion in *A. fumigatus* led to production of more gliotoxin than the wild-type strain (Winkelströter et al., 2015). By comparing transcriptomic and proteomic data, it was noted that most differentially regulated genes in the RNA-seq analyses did not show a change at translational level, including the genes involved in biosynthetic processes of neosartoricin/fumicycline.

Analysis of chromosomal patterns of gene expression in *ppzA* deletion mutant showed activated expression from both subcentromeric and subtelomeric genes during iron replete conditions, and subtelomeric genes become further activated under iron starvation. Subtelomeric regions are enriched in SM clusters, and their expression is regulated by specific activator genes, global regulators, changes at the chromatin level, and alteration of posttranslational protein modification (Macheleidt et al., 2016). Moreover, relative to wild type, mean expression in *ppzA* is weakly associated with chromosome size under iron replete conditions but highly correlated under iron starvation. Further analyses under varied challenging conditions are necessary to determine if the association between chromosome size and mean expression observed in *ppzA* is a general stress response or an effect specifically associated to iron starvation. In addition to the regulatory effects on iron acquisition affected by *ppzA* deletion, our proteomic data also corroborates that PpzA positively and negatively influences expression of specific *A. fumigatus* SM gene clusters, including gliotoxin, fumagillin, and pseurotin A. We found that GliT, a gliotoxin oxidoreductase required for gliotoxin biosynthesis, was present at higher levels in the *ppzA* mutant. Levels of five proteins involved in fumagillin biosynthetic processes and two implicated in pseurotin production were reduced in Δ*ppzA*. Corroborating this finding, HPLC analysis revealed that *ppzA* deletion in *A. fumigatus* causes a reduction in the production of fumagillin during iron starvation.

We investigated the influence of PpzA on MpkA and SakA phosphorylation upon iron starvation and oxidative stress. A previous study demonstrated that under iron starvation, *A. fumigatus* MpkA is activated by phosphorylation; it is localised in the nucleus and regulates the expression of genes involved in siderophore biosynthesis (Jain et al., 2011). In *A. fumigatus*, SakA is important for oxidative and osmotic stress as well as cell wall damage and heat shock (Bruder Nascimento et al., 2016). As shown here, MpkA phosphorylation triggered by iron starvation was not affected by PpzA. Furthermore, we observed that PpzA::GFP localised in the cytoplasm during nonstress conditions and upon iron stresses, it remained in the

cytoplasm (data not shown). Interestingly, our results demonstrated for the first time that SakA phosphorylation significantly increases during iron starvation in *A. fumigatus* wild-type strain. However, the SakA phosphorylation levels in the wild-type and *ppzA* mutant were similar in control and after iron starvation. These results suggest that PpzA may be acting downstream of MpkA and SakA upon iron starvation and oxidative stress.

PpzA immunoprecipitation identified 31 proteins that potentially interact with PpzA upon iron starvation. These interactions have to be validated through independent methods because they could be false positives. Some of interaction partners possibly are directly related to PpzA functions, whereas other proteins can be involved in some types of stress response, including regulation of the cell cycle, signal transduction, energy metabolism, and mitochondrial function. The proteins that could be directly associated to PpzA function include MpkA and the protein phosphatase type 1 activator (SdsA). We demonstrated by reciprocal Co-IP that PpzA and SdsA are interacting. Because MpkA phosphorylation was not affected by the absence of *ppzA*, it is likely that PpzA and MpkA could participate in a complex including other proteins that might redundantly regulate the MpkA activation during iron starvation. Because the ortholog of Afu1g04800 in *Saccharomyces cerevisiae* has protein phosphatase type 1 activator function (Bharucha et al., 2008; Hisamoto et al., 1995; MacKelvie, Andrews, Stark, et al., 1995; Pedelini et al., 2007) and Afu1g04800 interacts with PpzA, it is possible that this protein is the regulatory subunit of PpzA. In view of the fact that *sdsA* is an essential gene, it is possible that SdsA is also regulating other protein phosphatases.

In this work, we demonstrated that the PpzA was important for *A. fumigatus* virulence in a low-dose murine infection model. Similarly, a previous study reported that the *ppzA* mutant showed a defect in virulence in an experimental model of corneal infection in immunocompetent animals (Muszkieta et al., 2014). In *Candida albicans*, the lack of PPZ1 causes impaired virulence in a mouse virulence model (Adám et al., 2012). However, in *Fusarium graminearum*, the deletion of PPZ1 did not affect the organism virulence (Yun et al., 2015). Phagocytes produce reactive oxygen species, which is involved in the killing of *A. fumigatus*. However, none of the mutants that display a reactive oxygen species sensitivity defect consecutive to the deletion of superoxide dismutase, catalase, or the transcription factors Yap1 and Skn7 showed difference in virulence compared to wild-type strain in experimental murine aspergillosis models in immunocompromised animals (Lamarre, Ibrahim-Granet, Du, Calderone, & Latge, 2007; Lambou, Lamarre, Beau, Dufour, & Latge, 2010; Lessing et al., 2007; Paris et al., 2003). These observations suggest that the virulence defect of the *ppzA* mutant could not be solely due to its oxidative stress sensitivity. We showed that the *ppzA* mutant clearly has a lack of SM production in iron replete and iron starvation conditions. SMs play crucial roles as virulence factors during plants and animals infections (Scharf, Heinekamp, & Brakhage, 2014). Thus, our results suggest that PpzA is important for the fungal virulence probably through multiple mechanisms, such as low tolerance to oxidative stress and iron starvation, and the regulation of SM production.

Taken together, we show that, in *A. fumigatus*, PpzA is involved in regulation of genes ranging from those encoding transporters, oxidoreductases, and transcription factors, as well as genes involved in

siderophore and SM biosynthesis. PpzA might have an impact on SM gene cluster expression via regulation of signal transduction pathways and possibly through epigenetic modification of the chromatin structure. During iron starvation conditions, PpzA repressed the neosartoricin/fumicycline gene cluster and activated the biosynthesis of fumagillin and pseurotin. Thus, PpzA plays an important role at the interface between iron starvation, regulation of SM production, and pathogenicity in *A. fumigatus*. In order to chelate iron in our experiments, we have used a combination of BPS and ferrozine. Because BPS and ferrozine also chelate other metals (with lower affinity) such as zinc and copper, we cannot completely discard the possibility that some of the results observed here are due to shortage of metals other than iron. The possible involvement of PpzA and the identified genetic determinants in zinc and copper metabolism remains to be investigated.

4 | EXPERIMENTAL PROCEDURES

4.1 | Ethics statement

The principles that guide our studies are based on the Declaration of Animal Rights ratified by the UNESCO in January 27, 1978, in its eighth and 14th articles. All protocols used in this study were approved by the local ethics committee for animal experiments from the Campus of Ribeirão Preto, Universidade de São Paulo (Permit Number: 08.1.1277.53.6; Studies on the interaction of *A. fumigatus* with animals). All animals were housed in groups of five within individually ventilated cages and were cared for in strict accordance with the principles outlined by the Brazilian College of Animal Experimentation (Princípios Eticos na Experimentacãoo Animal—Colégio Brasileiro de Experimentacão Animal, COBEA) and Guiding Principles for Research Involving Animals and Human Beings, American Physiological Society. All efforts were made to minimise suffering. Animals were clinically monitored at least twice daily and humanely sacrificed if moribund (defined by lethargy, dyspnoea, hypothermia, and weight loss). All stressed animals were sacrificed by cervical dislocation.

4.2 | Strains, media, and growth conditions

The *A. fumigatus* parental strain used in this study was CEA17 (pyrG$^+$) *akuB*^{KU80} and and CEA17(pyrG$^-$) *akuB*^{KU80} (da Silva Ferreira et al., 2006) whereas the mutant strains were Δ*ppzA* (Winkelströter et al., 2015), Δ*ppzA::ppzA*$^+$, Δ*sdsA*, PpzA::GFP, PpzA::TAP, and SdsA::3xHA (this study). The media used were complete media composed of 2% *w/v* glucose; 0.5% *w/v* yeast extract; trace elements (YAG); and MM consisting of 1% glucose, trace elements, and salt solution (Käfer, 1977), pH 6.5, plus or minus 2% *w/v* agar. Strains were grown at 37 °C. For the experiments of iron starvation, we grew the strains in MM for 24 hr at 37 °C and transferred the mycelia to AMM (glucose 1% *w/v*, trace elements without FeSO) plus BPS 200 μM [Bathophenanthrolinedisulfonic acid (4,7-diphenyl-1,10 phenanthrolinedisulfonic acid)] and 3-(2-pyridyl)-5,6-bis(4-phenylsulfonic acid)-1,2,4-triazine (ferrozine) 300 μM for 1, 2, and 4 hr at 37 °C.

4.3 | Construction of the *A. fumigatus* mutants

The *A. fumigatus* phosphatase mutant *ppzA* was constructed by Winkelströter et al. (2015). The single gene deletion of the *ppzA* was complemented by co-transforming a DNA fragment (approximately 1 kb from each 5′- and 3′- flanking regions plus the ORF) together with the pHATα (Herrera-Estrella, Goldman, & Van Montagu, 1990) and selecting for hygromycin resistance in MM plates with 250 mg/ml of hygromycin B. PCR was used to confirm the reconstituted strain. The cassette for *sdsA* deletion was constructed by in vivo recombination in *S. cerevisiae* as previously described by Colot et al. (2006). Thus, approximately 2.0 kb from the 5′-UTR and 3′-UTR flanking region of the targeted ORF regions was selected for primer design. The primers 5F (sdsA pRS426 5fw) and 3R (sdsA pRS426 3rv) contained a short homologous sequence to the MCS of the plasmid pRS426. Both the 5- and 3-UTR fragments were PCR amplified from *A. fumigatus* genomic DNA (gDNA). The *pyrG* gene placed within the cassette as a prototrophic marker was amplified from pCDA21 plasmid. The deletion cassette was generated by transforming each fragment along with the plasmid pRS426 cut with *Bam*HI/*Eco*RI into the *S. cerevisiae* strain SC94721 using the lithium acetate method (Schiestl & Gietz, 1989). The DNA from the transformants was extracted by the method described by Goldman et al. (2003). The cassette was PCR amplified from these plasmids utilising TaKaRa Ex Taq™ DNA Polymerase (Clontech Takara Bio) and used for *A. fumigatus* transformation. Southern blot analysis demonstrated that the transformation cassette had integrated homologously at the targeted loci (Figure S4). To generate the PpzA::GFP strain, the *ppzA* ORF was cloned in frame with the GFP gene. The construct links GFP to the C-terminus of PpzA and is separated by four additional codons that, after translation, produce a four-amino-acid linker (glycine-threonine-arginine-glycine; Teepe, Loprete, He, Hoggard, & Hill, 2007). The *S. cerevisiae* in vivo recombination system was used for production of the transformation cassette. First, the *ppzA* ORF and 503 BP of the 5′-UTR flanking region were amplified from gDNA of the wild-type strain by the use of the primers ppzA pRS426 5Fw and ppzA SPACER GFP Rv. The stop codon of the *ppzA* gene was omitted in this construction. The GFP ORF was amplified from the pMCB17apx plasmid (provided by Vladimir P. Efimov) by the use of the primers Spacer GFP Fw and GFP VE3' AF. The *pyrG* selective marker was PCR amplified from the pCDA21 plasmid using the primers GFP pyrG Fw and pyrG Rv. The amplification of the 3′-UTR (606 BP) used the Afu ppzA 3Fw and Afu ppzA 3Rv primers. The PCR-amplified cassette was transformed into the *A. fumigatus* wild-type strain. PCR was used to confirm the mutant strain (Figure S5). To generate the *sdsA::3xHA::pyrG* fusion fragment, a 1.6-Kb portion of DNA consisting of the *sdsA* ORF and 5′ UTR region, along with a 1-Kb segment of DNA consisting of the 3′ UTR flanking region were amplified with primers sdsA pRS426 5fw(3xHA)/sdsA orf LINKER 3HA rv and sdsA 3utr pyrG 3fw/sdsA pRS426 3rv, respectively, from CEA17 gDNA. The 2.7-kb *3xHA::pyrG* fusion was amplified with primers OZG916/OZG964 from the pOB430 plasmid. The cassette was generated by transforming each fragment along with the plasmid pRS426 cut with *Bam*HI/*Eco*RI into the *S. cerevisiae* strain. This cassete was then transformed into the CEA17 strain and verification of SdsA tagging was confirmed via PCR reaction (Figure S6). The primers used above are described in Table S10.

4.4 | RNA extraction and real-time PCR reactions

Posttreatment, mycelia were harvested by filtration, washed twice with H_2O, and immediately frozen in liquid nitrogen. For total RNA isolation, mycelia were ground in liquid nitrogen. Total RNA was extracted using Trizol (Invitrogen). The integrity of the RNA isolated from each treatment was analysed using the Agilent 2100 Bioanalyzer system. For real-time PCR experiments, RNase free DNase I treatment was carried out as previously described by Semighini, Marins, Goldman, and Goldman (2002). RNASeq data (see below) was exploited to select genes for normalisation of the qPCR data, applying the method of Yim et al. (2015). Briefly, genes with a coefficient of variation smaller than 20%, behaving in a normally distributed manner, and with large expression values (FPKM), were selected. After experimental validation, gene AFUB_002930/Afu1g02550 (tubulin alpha-1 subunit) was selected. Twenty micrograms of total RNA was treated with DNase, purified using a RNeasy kit (Qiagen), and cDNA was generated using the SuperScript III First Strand Synthesis system (Invitrogen) with oligo(dT) primers, according to the manufacturer's instructions. RT-qPCR was performed for each primer pair using known amounts of target obtained by serial dilutions of gDNA as the template over several orders of magnitude. The initial template amount used in the parallel reaction mixtures was estimated, using 30 Mb as the *Aspergillus nidulans* (*A. nidulans*) genome size. A linear relationship was obtained by plotting the threshold cycle against the logarithm of known amount of initial template. The equation of the line that best fits the data was determined by regression analysis. The R^2 value was calculated for each data set to estimate the accuracy of the real-time PCR as a quantification method. The number of target copies contained in an unknown sample was determined by extrapolation from the linear regression of the standard curve obtained for each primer. In all experiments, appropriate negative controls containing no template DNA or RNA were subjected to the same procedure to exclude or detect any possible contamination or carryover. Each sample was repeated at least three times. All reaction mixtures were analysed by agarose gel electrophoresis to confirm that only one PCR product was synthesised. The results were normalised using the C_Ts obtained for the gene AFUB_002930/Afu1g02550 (tubulin alpha-1 subunit) RNA amplifications run on the same plate. All the PCR reactions were performed using an ABI 7500 Fast Real-Time PCR System (Applied Biosystems) and SYBR® Green PCR Master Mix (Applied Biosystems). The primer sets for the analyses are listed in Table S10.

4.5 | RNA sequencing

Wild-type (CEA17) and Δ*ppzA* (5 × 10⁶ spores) were inoculated in MM for 24 hr at 37 °C and transferred to AMM (glucose 1% *w/v*, trace elements without FeSO) plus BPS 200 μM [Bathophenanthrolinedisulfonic acid (4,7-diphenyl-1,10 phenanthrolinedisulfonic acid)] and 3-(2-pyridyl)-5,6-bis(4-phenylsulfonic acid)-1,2,4-triazine (ferrozine) 300 μM for 1 or 2 hr at 37 °C. Each condition was evaluated with three biological replicates. Mycelia were harvested, frozen in liquid nitrogen, and ground by mortar and pestle for total RNA isolation. Total RNA was extracted using Trizol (Invitrogen), treated with RNase-free DNase I (Fermentas), and purified using an RNAeasy Kit (Qiagen) according to the manufacturer's instructions. The RNA from each treatment was quantified using a NanoDrop and Qubit fluorometer and analysed using an Agilent 2100 Bioanalyzer system to assess the integrity of the RNA. RNA integrity number (RIN) was calculated; RNA samples had an RIN = 9.0–9.5.

Illumina TruSeq Stranded mRNA Sample Preparation kit was used. Briefly, polyA containing mRNA molecules were selected using polyT oligo-attached magnetic beads. Fragmentation and library preparation were done using divalent cations and thermal fragmentation. First strand cDNA synthesis was performed using reverse transcriptase (Superscript II) and random primers. This was followed by second strand cDNA synthesis using DNA Polymerase I and RNase H and dUTP in place of dTTP. AMPure XP beads were used to separate the dscDNA from the second strand. At the end of this process, blunt-ended cDNA was obtained to which a single "A" nucleotide was added at the 3′ end to prevent them from ligating to one another during the adapter ligation reaction. A corresponding single "T" nucleotide on the 3′ end of the adapter provided a complementary overhang for ligating the adapter to the fragment. The products were then purified and enriched using a PCR to selectively enrich those DNA fragments that have adapter molecules on both ends and to amplify the amount of DNA in the library. The PCR was performed with a PCR Primer Cocktail from the Illumina kit that anneals to the ends of the adapters. The data discussed in this publication have been deposited in NCBI's Gene Expression Omnibus (Edgar, Domrachev, & Lash, 2002) and are accessible through GEO Series accession number GSE97495 (https://www.ncbi.nlm.nih.gov/geo/query/acc.cgi?acc=GSE97495). Underlying raw short reads are associated to the BioProject PRJNA381768 (https://www.ncbi.nlm.nih.gov/bioproject/PRJNA381768). To examine broad chromosomal expression patterns, raw read counts were normalised to equal number for each replicate sample, then wild-type and Δ*ppzA* values were quantile normalised. Where A1163 chromosomes have not been fully assembled, chromosomal structure was inferred from the Sybil alignment of A1163 to Af293 available from AspGD (http://www.aspgd.org/).

4.6 | LC-MS qualitative SM analysis

Wild-type (CEA17), Δ*ppzA*, and the complemented strains (5 × 10⁷ spores) were grown in MM for 24 hr, 37 °C, 200 rpm. Mycelia were transferred to MM without iron plus BPS 200 μM [Bathophenanthrolinedisulfonic acid (4,7-diphenyl-1,10 phenanthrolinedisulfonic acid)] and 3-(2-pyridyl)-5,6-bis(4-phenylsulfonic acid)-1,2,4-triazine (ferrozine) 300 μM for 2 and 4 hr, respectively. Each condition was carried out in triplicate. Extractions and analytic analysis of SMs were performed according to Mattern et al. (2015). For initial analysis, the LTQ XL Linear Ion Trap (Thermo Fisher Scientific, Dreieich, Germany) was used along with differential analysis using the Sieve 2.1 (Thermo Fisher Scientific, Dreieich, Germany) software. This was then confirmed using a Bruker micrOTOF-Q (Bruker, Leipzig, Germany) mass spectrometer coupled to an Agilent 1260 Infinity HPLC (Agilent, Waldbronn, Germany). HPLC method was the same used in Mattern et al. (2015).

4.7 | Label-free quantitative proteomics

Wild type (CEA17) and $\Delta ppzA$ (5×10^7 conidia) were grown in MM for 24 hr, 37 °C, 200 rpm. Mycelia were transferred to MM without iron plus BPS 200 µM [Bathophenanthrolinedisulfonic acid (4,7-diphenyl-1,10 phenanthrolinedisulfonic acid)] and 3-(2-pyridyl)-5,6-bis(4-phenylsulfonic acid)-1,2,4-triazine (ferrozine) 300 µM for 2 and 4 hr, respectively. Each condition was carried out in triplicate. Control samples were also prepared for each strain. The mycelia (18 × samples) were harvested with Miracloth, dried between tissue, and snap-frozen in liquid nitrogen. The culture supernatants were also collected. The mycelia were ground in liquid nitrogen and suspended in lysis buffer (100 mM Tris-HCl, 50 mM NaCl, 20 mM EDTA, 10% (v/v) glycerol, 1 mM PMSF, 1 µg/ml pepstatin A pH 7.5). The mycelia were lysed using the sonication probe and clarified by centrifugation. The resulting clarified lysates were precipitated using TCA/acetone and resuspended in 8 M urea. Samples were reduced (DTT) and alkylated (IAA) prior to digestion with sequencing grade trypsin combined with ProteaseMax surfactant. Samples were acidified following overnight digestion, and the peptide samples were cleaned using C18 spin columns. The resultant peptide samples were analysed on a Q-Exactive mass spectrometer coupled to a DionexRSLCnano. The gradient ran from 4% to 35% B over 120 min, and data were collected using a Top15 method for MS/MS scans. Data analysis was performed using MaxQuant software, with Andromeda used for database searching and Perseus used to organise the data (Dolan et al., 2014; Owens et al., 2015).

4.8 | Immunoblot analysis

To assess the phosphorylation status of MpkA and SakA^{HOG1}, fresh harvested spores (1×10^7) of the wild type and $\Delta ppzA$ were inoculated in 50-ml liquid MM at 37 °C for 24 hr (160 rpm). The mycelia were transferred to MM without iron plus BPS 200 µM [Bathophenanthrolinedisulfonic acid (4,7-diphenyl-1,10 phenanthrolinedisulfonic acid)] and 3-(2-pyridyl)-5,6-bis(4-phenylsulfonic acid)-1,2,4-triazine (ferrozine) 300 µM. This treatment was performed for 10, 30, 60, and 120 min, and, then, the mycelia were frozen and ground in liquid nitrogen. For protein extraction, 0.5-ml lysis buffer (Valiante et al., 2009) containing 10% (v/v) glycerol, 50 mM Tris-HCl pH 7.5, 1% (v/v) Triton X-100, 150 mM NaCl, 0.1% (w/v) SDS, 5 mM EDTA, 50 mM sodium fluoride, 5 mM sodium pyrophosphate, 50 mM b-glycerophosphate, 5 mM sodium orthovanadate, 1 mM PMSF, and 1X Complete Mini-protease inhibitor (Roche Applied Science) were added to the ground mycelium. Extracts were centrifuged at 20,000 g for 40 min at 4 °C. The supernatants were collected, and the protein concentrations were determined using the Bradford method (BioRad). Approximately 50 µg of protein from each sample were resolved in a 12% (w/v) SDS-PAGE and transferred polyvinylidene difluoride membranes using the iBlot® 2 Dry Blotting System (Thermo Scientific™). The phosphorylation state of MpkA was examined using a rabbit polyclonal IgG antibody against dually phophorylated p44-42 MAPK (Cell Signaling Technology) and the phosphorylation of SakA was examined using a rabbit polyclonal IgG antibody against phophorylated p38 MAPK (Cell Signaling

Technology), respectively. Primary antibodies were detected using an Anti-rabbit IgG, horseradish peroxidase (HRP)-linked Antibody #7074 (Cell Signaling Technologies). Chemoluminescent detection was achieved using the Super Signal West Pico Chemiluminescent Substrate (Thermo Scientific™) and the images generated were subjected to densitometric analysis using the ImageJ software (http://rsbweb.nih.gov/ij/index.html). The mpkA and sakA phosphorylated signal were normalised by ponceau staining.

4.9 | Construction of the PpzA TAP-tagged strain and TAP-tag protein purification and identification by LC-MS/MS

Transformation of the *ppzA::tap::hph* phusion fragment into an *A. fumigatus* wild-type strain (CEA17) via homologous recombination yielded the strain, containing a TAP-tag at the C-terminus of *ppzA* gene. To generate the *ppzA::tap::hph* fusion fragment, a 2.5-Kb portion of DNA consisting of the *ppzA* ORF and 5′ UTR region, along with a 1.5-Kb segment of DNA consisting of the 3′ UTR flanking region were amplified with primers MUL1/MUL3 and MUL4/MUL6, respectively, from CEA17 gDNA. The 3.4-kb *tap::hph* fusion was amplified with primers OZG916/OZG964 from the pOB446 plasmid. Subsequently, the amplicons were cloned into a pUC19 plasmid containing a *Sma*I restriction site by HD in-fusion cloning to generate the pMU1 plasmid. The 7.2-kb *ppzA::tap::hph* fused fragment was amplified from the pMU1 plasmid using the primers MUL2/MUL5. This fragment was then transformed into the CEA17 strain and verification of PpzA tagging was confirmed via Southern hybridisation (Figure S4).

To precipitate TAP-tag-labelled PpzA, protein crude extracts were prepared from cultures incubated with or without iron starvation as follows. A total of 1×10^7 spores were used to inoculate 200 ml of liquid culture and incubated for 24 hr at 37 °C, with shaking. After this, the mycelia were transferred to MM without iron plus BPS 200 µM [Bathophenanthrolinedisulfonic acid (4,7-diphenyl-1,10 phenanthrolinedisulfonic acid)] and 3-(2-pyridyl)-5,6-bis(4-phenylsulfonic acid)-1,2,4-triazine (ferrozine) 300 µM for 2 and 4 hr, respectively. Protein purification was performed as reported previously (Bayram et al., 2012). Briefly, samples were frozen with liquid nitrogen, ground, and resuspended in 5 ml of protein extraction buffer (50 mM Tris [pH 7.5], 100 mM KCl, 10 mM MgCl2, 0.1% NP-40, 10% glycerol, 20 mM b-glycerophosphate, 2 mM Na3VO4, 5 mM NaF, 0.5 mM phenylmethylsulfonylfluoride [PMSF], 1 mM benzamidine, 1 mM EGTA, 1 mM dithiothreitol [DTT], and 2× protease inhibitors [Roche]). After two centrifugation steps at 4 °C, the supernatant was transferred to a new tube and incubated at 4 °C with 300 µl of TAP-protein agarose slurry (Novagen) per 100 mg of protein in a rotary shaker for 2 hr. After this, TAP-protein beads were collected by centrifugation and the supernatant was discarded. Beads were washed twice and resuspended in 1 ml of protein extraction buffer. Protein extraction was performed twice using 1 ml of extraction buffer. Purified supernatant was incubated with 50 µl of 3× Laemmli gel loading dye, boiled at 95 °C for 10 min, and stored at −80 °C until used. Liquid chromatography–tandem mass spectrometry (LC-MS/MS) protein identification was done as described by Bayram et al. (2008).

4.10 | Co-IP with GFP-trap and anti-HA magnetic beads

To perform Co-IP assays, C-terminal HA-tagged SdsA strain was generated in the PpzA::GFP background. GFP-Trap Co-IP experiments were performed in the same way as the previously described GFP-Trap immunoprecipitation experiments (Ries, Beattie, Espeso, Cramer, & Goldman, 2016). To perform reciprocal Co-IP assays, C-terminal HA-tagged SdsA strain was used. Briefly, mycelia were frozen with liquid nitrogen and ground, and 500 mg was resuspended in 1 ml of B250 buffer (Bayram et al., 2012). Samples were centrifuged at maximum speed for 10 min at 4 °C. Supernatant was removed, and a Bradfordassay (BioRad) was carried out to measure protein content. The same amount of protein for each sample was added to 20 µl of Dynabeads Protein A (Thermo Fisher Scientific) previously incubated with monoclonal anti-HA antibody (Sigma). The resin was washed three times with resuspension buffer prior to incubation. Cell extracts and resin then were incubated with shaking at 4 °C for 2 hr. After incubation, the resin was washed three times in resuspension buffer by placing the tube in a DynaMag™ magnet. To release the proteins from the resin, samples were incubated with sample buffer and boiled at 98 °C for 5 min. Proteins were transferred from a 10% SDS-PAGE gel onto a nitrocellulose membrane for a Western blot assay using a Trans-Blot turbo transfer system (Bio-Rad). GFP-tagged PpzA was detected using a rabbit anti-GFP antibody (Abcam) at 1:2,000 dilution and a goat anti-rabbit IgG HRP antibody (Cell Signaling Technology) at 1:10,000 dilution. For the HA-tagged SdsA, a mouse monoclonal anti-HA antibody (Sigma) was used at 1:2,000 dilution as a primary antibody followed by an anti-mouse IgG HRP conjugate (Cell Signaling Technology) used at 1:10,000 dilution as a secondary antibody.

4.11 | Murine model of pulmonary aspergillosis, lung histopathology, and fungal burden

Outbreed female mice (BALB/c strain; body weight, 20 to 22 g) were housed in vented cages containing five animals. Mice were immunosuppressed with cyclophosphamide (150 mg/kg of body weight), which was administered intraperitoneally on Days −4, −1, and 2 prior to and post infection. Hydrocortisonacetate (200 mg/kg body weight) was injected subcutaneously on Day −3. *A. fumigatus* strains were grown on YAG for 2 days prior to infection. Fresh conidia were harvested in PBS and filtered through a Miracloth (Calbiochem). Conidial suspensions were spun for 5 min at 3,000×*g*, washed three times with PBS, counted using a haemocytometer, and resuspended at a concentration of 5.0×10^6 conidia/ml. The viability of the administered inoculum was determined by incubating a serial dilution of the conidia on YAG medium, at 37 °C. Mice were anaesthetised by halothane inhalation and infected by intranasal instillation of 1.0×10^5 conidia in 20 µl of PBS. As a negative control, a group of five mice received PBS only. Mice were weighed every 24 hr from the day of infection and visually inspected twice daily. The statistical significance of the comparative survival values was calculated using log rank analysis and the Prism statistical analysis package.

To investigate fungal burden in murine lungs, mice were immunosuppressed with cyclophosphamide (150 mg/kg of body weight), which was administered intraperitoneally on Days −4 and −1, whereas hydrocortisonacetate was injected subcutaneously (200 mg/kg) on Day-3. Five mice per group were intranasally inoculated with 1×10^6 conidia/ 20 µl of suspension. A higher inoculum, in comparison to the survival experiments, was used to increase fungal DNA detection. Animals were sacrificed 72 hr postinfection, and the lungs were harvested and immediately frozen in liquid nitrogen. Samples were homogenised by vortexing with glass beads for 10 min, and DNA was extracted via the phenol-chloroform method. DNA quantity and quality were assessed using a NanoDrop 2000 spectrophotometer (Thermo Scientific). At least 500 µg of total DNA from each sample was used for quantitative real-time PCRs. A primer and a Lux probe (Invitrogen) were used to amplify the 18S rRNA region of *A. fumigatus* (primer, 5′-CTTAAATAGCCCGGTCCGCATT-3′; probe, 5′-CATCAC AGACCTGTTATTGCCG-3′) and an intronic region of mouse GAPDH (glyceraldehyde-3-phosphate dehydrogenase; primer, 5′-CGAGGG ACTTGGAGGACACAG-3′; probe, 5′-GGGCAAGGCTAAAGGTCAG CG-3′). Six-point standard curves were calculated using serial dilutions of gDNA from all the *A. fumigatus* strains used and the uninfected mouse lung. Fungal and mouse DNA quantities were obtained from the threshold cycle (*CT*) values from an appropriate standard curve. Fungal burden was determined as the ratio between picograms of fungal and micrograms of mouse DNA.

For the histopathology, the animals were also sacrificed 72 hr postinfection; the lungs were removed and fixed for 24 hr in 3.7% formaldehyde-PBS. Samples were washed several times in 70% alcohol before dehydration in a series of alcohol solutions of increasing concentrations. Finally, the samples were diafanized in xylol and embedded in paraffin. For each sample, sequential 5-µm-thick sections were collected on glass slides and stained with Gomori methenamine silver (GMS) or haematoxylin and eosin (HE) stain following standard protocols. Briefly, sections were deparaffinised, oxidised with 4% chromic acid, stained with methenamine silver solution, and counterstained with picric acid. For HE staining, sections were deparaffinised and stained first with haematoxylin and then with eosin. All stained slides were immediately washed, preserved with mounting medium, and sealed with a coverslip. Microscopic analyses were done using an Axioplan 2 imaging microscope (Zeiss) at the stated magnifications under bright-field conditions.

ORCID

Gustavo H. Goldman http://orcid.org/0000-0002-2986-350X

REFERENCES

Adám, C., Erdei, E., Casado, C., Kovács, L., González, A., Majoros, L., ... Dombrádi,, V. (2012). Protein phosphatase CaPpz1 is involved in cation homeostasis, cell wall integrity and virulence of Candida albicans. Microbiology, 158, 1258–1267.

Alves de Castro, P., Dos Reis, T. F., Dolan, S. K., Oliveira Manfiolli, A., Brown, N. A., Jones, G. W., ... Goldman, G. H. (2016). The Aspergillus fumigatus SchA(SCH9) kinase modulates SakA(HOG1) MAP kinase activity and it is essential for virulence. Molecular Microbiology, 102, 642–671.

Baldin, C., Valiante, V., Krüger, T., Schafferer, L., Haas, H., Kniemeyer, O., & Brakhage, A. A., et al. (2015). Comparative proteomics of a TOR inducible Aspergillus fumigatus mutant reveals involvement of the TOR kinase in iron regulation. Proteomics, 15, 2230–2243.

Bayram, O., Bayram, O. S., Valerius, O., Jöhnk, B., & Braus, G. H. (2012). Identification of protein complexes from filamentous fungi with tandem affinity purification. Methods in Molecular Biology, 944, 191–205.

Bayram, O., Krappmann, S., Ni, M., Bok, J. W., Helmstaedt, K., Valerius, O., ... Braus, G. H. (2008). VelB/VeA/LaeA complex coordinates light signal with fungal development and secondary metabolism. Science, 320, 1504–1506.

Berthier, E., Lim, F. Y., Deng, Q., Guo, C. J., Kontoyiannis, D. P., Wang, C. C., ... Keller, N. P. (2013). Low-volume tool box for the discovery of immunosuppressive fungal secondary metabolites. PLoS Pathogens, 9. e1003289

Bharucha, J. P., Larson, J. R., Gao, L., Daves, L. K., Tatchell, K., et al. (2008). Ypi1, a positive regulator of nuclear protein phosphatase type 1 activity in Saccharomyces cerevisiae. Molecular Biology of the Cell, 19(3), 1032–1045.

Bok, J. W., Chung, D., Balajee, S. A., Marr, K. A., Andes, D., Nielsen, K. F., ... Keller, N. P. (2006). GliZ, a transcriptional regulator of gliotoxin biosynthesis, contributes to Aspergillus fumigatus virulence. Infection and Immunity, 74, 6761–6768.

Brakhage, A. A. (2005). Systemic fungal infections caused by Aspergillus species: Epidemiology, infection process and virulence determinants. Current Drug Targets, 6, 875–886.

Brakhage, A. A. (2013). Regulation of fungal secondary metabolism. Nature Reviews. Microbiology, 11, 21–32.

Brodhagen, M., & Keller, N. P. (2006). Signalling pathways connecting mycotoxin production and sporulation. MolPlant Pathol, 7, 285–301.

Bruder Nascimento, A. C., Dos Reis, T. F., de Castro, P. A., Hori, J. I., Bom, V. L., de Assis, L. J., ... Goldman, G. H. (2016). Mitogen activated protein kinases SakA(HOG1) and MpkC collaborate for Aspergillus fumigatus virulence. Molecular Microbiology, 100, 841–859.

Cairo, G., Bernuzzi, F., & Recalcati, S. (2006). A precious metal: Iron, an essential nutrient for all cells. Genes & Nutrition, 1, 25–39.

Carberry, S., Molloy, E., Hammel, E., O'Keeffe, G., Jones, G. W., ... Doyle, S. (2012). Gliotoxin effects on fungal growth: Mechanisms and exploitation. Fungal Genetics and Biology, 49, 302–312.

Cassat, J. E., & Skaar, E. P. (2013). Iron in infection and immunity. Cell Host & Microbe, 13(637), 509–519.

Chotirmall, S. H., Mirkovic, B. G., Lavelle, M., & McElvaney, N. G. (2014). Immunoevasive Aspergillus virulence factors. Mycopathologia, 178, 363–370.

Colot, H. H., Park, G., Turner, G. E., Ringelberg, O., Crew, C. M., ... Dunlap, J. C. (2006). A high throughput gene knockout procedure for Neurospora reveals functions for multiple transcription factors. Proc Nat Acad Sci USA, 103, 10352–10357.

Dagenais, T. R., & Keller, N. P. (2009). Pathogenesis of Aspergillus fumigatus in invasive Aspergillosis. Clinical Microbiology Reviews, 22, 447–465.

Ding, S., Mehrabi, R., Koten, C., Kang, Z., Wei, Y., Seong, K., ... Xu, J. R. (2009). Transducin beta-like gene FTL1 is essential for pathogenesis in Fusarium graminearum. Eukaryotic Cell, 8, 867–876.

Dolan, S. K., Owens, R. A., O'Keeffe, G., Hammel, S., Fitzpatrick, D. A., Jones, G. W., & Doyle, S. (2014). Regulation of nonribosomal peptide synthesis: bis-thiomethylation attenuates gliotoxin biosynthesis in Aspergillus fumigatus. Chemistry Biology, 21, 999–1012.

Drakesmith, H., & Prentice, A. (2008). Viral infection and iron metabolism. Nature Reviews. Microbiology, 6, 541–552.

Edgar, R., Domrachev, M., & Lash, A. E. (2002). Gene expression omnibus: NCBI gene expression and hybridization array data repository. Nucleic Acids Research, 30, 207–210.

Eisendle, M., Oberegger, H., Zadra, I., & Haas, H. (2003). The siderophore system is essential for viability of Aspergillus nidulans: Functional analysis of two genes encoding l-ornithine N 5-monooxygenase (sidA) and a non-ribosomal peptide synthetase (sidC). Molecular Microbiology, 49, 359–375.

Frisvad, J. C., Rank, C., Nielsen, K. F., & Larsen, T. O. (2009). Metabolomics of Aspergillus fumigatus. Medical Mycology, 47(Suppl 1), S53–S71.

Ganz, T. (2009). Iron in innate immunity: Starve the invaders. Current Opinion in Immunology, 21(635), 63–67.

Gauthier, G. M., Sullivan, T. D., Gallardo, S. S., Brandhorst, T. T., Vanden Wymelenberg, A. J., Cuomo, C. A. ... Klein, B. S. (2010). SREB, a GATA transcription factor that directs disparate fates in Blastomyces dermatitidis including morphogenesis and siderophore biosynthesis. PLoS Pathogens, 6. e1000846

Gehrke, A., Heinekamp, T., Jacobsen, I. D., & Brakhage, A. A. (2010). Heptahelical receptors GprC and GprD of Aspergillus fumigatus are essential regulators of colony growth, hyphal morphogenesis, and virulence. Applied and Environmental Microbiology, 76, 3989–3998.

Goldman, G. H., dos Reis Marques, E., Duarte Ribeiro, D. C., de Souza Bernardes, L. A., Quiapin, A. C., Vitorelli, P. M., ... Goldman, M. H. (2003). Expressed sequence tag analysis of the human pathogen Paracoccidioides brasiliensis yeast phase: Identification of putative homologues of Candida albicans virulence and pathogenicity genes. Eukaryotic Cell, 2, 34–48.

Grahl, N., Dinamarco, T. M., Willger, S. D., Goldman, G. H., & Cramer, R. A. (2012). Aspergillus fumigatus mitochondrial electron transport chain mediates oxidative stress homeostasis, hypoxia responses and fungal pathogenesis. Molecular Microbiology, 84, 383–399.

Greenshields, D. L., Liu, G., Feng, J., Selvaraj, G., & Wei, Y. (2007). The siderophore biosynthetic gene SID1, but not the ferroxidase gene FET3, is required for full Fusarium graminearum virulence. Molecular Plant Pathology, 8, 411–421.

Grosse, C., Heinekamp, T., Kniemeyer, O., Gehrke, A., & Brakhage, A. A. (2008). Protein kinase A regulates growth, sporulation, and pigment formation in Aspergillus fumigatus. Applied and Environmental Microbiology, 74, 4923–4933.

Gsaller, F., Hortschansky, P., Beattie, S. R., Klammer, V., Tuppatsch, K., Lechner, B. E., ... Haas, H. (2014). The Janus transcription factor HapX controls fungal adaptation to both iron starvation and iron excess. The EMBO Journal, 33, 2261–2276.

Haas, H. (2003). Molecular genetics of fungal siderophore biosynthesis and uptake: The role of siderophores in iron uptake and storage. Applied Microbiology and Biotechnology, 62, 316–330.

Hagiwara, D., Suzuki, S., Kamei, K., Gonoi, T., & Kawamoto, S. (2014). The role of AtfA and HOG MAPK pathway in stress tolerance in conidia of Aspergillus fumigatus. Fungal Genetics and Biology, 73, 138–149.

Heinekamp, T., Thywissen, A., Macheleidt, J., Keller, S., Valiante, V., & Brakhage, A. A. (2012). Aspergillus fumigatus melanins: Interference with the host endocytosis pathway and impact on virulence. Frontiers in Microbiology, 3, 440.

Herrera-Estrella, A., Goldman, G. H., & Van Montagu, M. (1990). High-efficiency transformation system for the biocontrol agents, Trichoderma spp. Molecular Microbiology, 4, 839–843.

Hicks, J. K., Yu, J. H., Keller, N. P., & Adams, T. H. (1997). Aspergillus sporulation and mycotoxin production both require inactivation of the FadA G alpha protein-dependent signaling pathway. The EMBO Journal, 16, 4916–4923.

Hisamoto, N., Frederick, D. L., Sugimoto, K., Tatchell, K., & Matsumoto, K. (1995). The EGP1 gene may be a positive regulator of protein phosphatase type 1 in the growth control of Saccharomyces cerevisiae. Molecular and Cellular Biology, 15, 3767–3776.

Hissen, A. H., Wan, A. N., Warwas, M. L., Pinto, L. J., & Moore, M. M. (2005). The *Aspergillus fumigatus* siderophore biosynthetic gene *sidA*, encoding L-ornithine N5-oxygenase, is required for virulence. *Infection and Immunity*, *73*, 5493–5503.

Hoffmeister, D., & Keller, N. P. (2007). Natural products of filamentous fungi: Enzymes, genes, and their regulation. *Natural Product Reports*, *24*, 393–416.

Hohl, T. M., & Feldmesser, M. (2007). *Aspergillus fumigatus*: Principles of pathogenesis and host defense. *Eukaryotic Cell*, *6*, 1953–1963.

Hortschansky, P., Eisendle, M., Al-Abdallah, Q., Schmidt, A. D., Bergmann, S., Thön, M., ... Haas, H. (2007). Interaction of HapX with the CCAAT-binding complex—A novel mechanism of gene regulation by iron. *The EMBO Journal*, *26*, 3157–3168.

Hwang, L. H., Grouph, E., Gilmore, S. A., & Sil, A. (2012). SRE1 regulates irondependent and -independent pathways in the fungal pathogen *Histoplasma capsulatum*. *Eukaryotic Cell*, *11*, 16–25.

Jahn, B., Langfelder, K., Schneider, U., Schindel, C., & Brakhage, A. A. (2002). PKSP-dependent reduction of phagolysosome fusion and intracellular kill of *Aspergillus fumigatus* conidia by human monocyte-derived macrophages. *Cellular Microbiology*, *4*, 793–803.

Jain, R., Valiante, V., Remme, N., Docimo, T., Heinekamp, T., Hertweck, C., ... Brakhage, A. A. (2011). The MAP kinase MpkA controls cell wall integrity, oxidative stress response, gliotoxin production and iron adaptation in Aspergillus fumigatus. *Molecular Microbiology*, *82*, 39–53.

Jung, W. H., & Kronstad, J. W. (2008). Iron and fungal pathogenesis: A case study with *Cryptococcus neoformans*. *Cellular Microbiology*, *10*, 277–284.

Käfer, E. (1977) The anthranilate synthetase enzyme complex and the trifunctional trpC gene of *Aspergillus*. *Can J Genet Cytol*, *19*, 723–38.

Khan, F. A., Fisher, M. A., & Khakoo, R. A. (2007). Association of hemochromatosis with infectious diseases: Expanding spectrum. *International Journal of Infectious Diseases*, *11*, 482–487.

König, C. C., Scherlach, K., Schroeckh, V., Horn, F., Nietzsche, S., Brakhage, A. A., & Hertweck, C. (2013). Bacterium induces cryptic meroterpenoid pathway in the pathogenic fungus *Aspergillus fumigatus*. *Chembiochem*, *14*, 938–942.

Kosman, D. J. (2013). Iron metabolism in aerobes: Managing ferric iron hydrolysis and ferrous iron autoxidation. *Coordination Chemistry Reviews*, *257*, 210–217.

Lamarre, C., Ibrahim-Granet, O., Du, C., Calderone, R., & Latge, J. P. (2007). Characterization of the SKN7 ortholog of *Aspergillus fumigatus*. *Fungal Genetics and Biology*, *44*, 682–690.

Lambou, K., Lamarre, C., Beau, R., Dufour, N., & Latge, J. P. (2010). Functional analysis of the superoxide dismutase family in *Aspergillus fumigatus*. *Molecular Microbiology*, *75*, 910–923.

Lan, C. Y., Rodarte, G., Murillo, L. A., Jones, T., Davis, R. W., Dungan, J., Newport, G., & Agabian, N. (2004). Regulatory networks affected by iron availability in *Candida albicans*. *Molecular Microbiology*, *53*, 1451–1469.

Latgé, J. (1999). *Aspergillus fumigatus* and Aspergillosis. *Clinical Microbiology Reviews*, *12*, 310–350.

Leiter, É., González, A., Erdei, É., Casado, C., Kovács, L., Ádám, C., ... Dombrádi, V. (2012). Protein phosphatase Z modulates oxidative stress response in fungi. *Fungal Genetics and Biology*, *49*, 708–716.

Lessing, F., Kniemeyer, O., Wozniok, I., Loeffler, J., Kurzai, O., Haertl, A., & Brakhage, A. A. (2007). The *Aspergillus fumigatus* transcriptional regulator AfYap1 represents the major regulator for defense against reactive oxygen intermediates but is dispensable for pathogenicity in an intranasal mouse infection model. *Eukaryotic Cell*, *6*, 2290–2302.

Litwin, C. M., & Calderwood, S. B. (1993). Role of iron in regulation of virulence genes. *Clinical Microbiology Reviews*, *6*, 137–149.

Macheleidt, J., Mattern, D. J., Fischer, J., Netzker, T., Weber, J., Schroeckh, V., ... Brakhage, A. A. (2016). Regulation and role of fungal secondary metabolites. *Annual Review of Genetics*, *50*, 371–392.

MacKelvie, S. H., Andrews, P. D., Stark, M. J. (1995). The *Saccharomyces cerevisiae* gene SDS22 encodes a potential regulator of the mitotic function of yeast type 1 protein phosphatase. *Molecular and Cellular Biology*, *15*, 3777–3785.

Magnani, T., Soriani, F. M., Martins, V. d. P., Policarpo, A. C., Sorgi, C. A., Faccioli, L. H., ... Uyemura, A. S. (2008). Silencing of mitochondrial alternative oxidase gene of Aspergillus fumigatus enhances reactive oxygen species production and killing of the fungus by macrophages. *Journal of Bioenergetics and Biomembranes*, *40*, 631–636.

Mattern, D. J., Schoeler, H., Weber, J., Novohradska, S., Kraibooj, K., Dahse, H., ... Brakhage, A. A. (2015). Identification of the antiphagocytic trypacidin gene cluster in the human-pathogenic fungus *Aspergillus fumigatus*. *Applied Microbiology and Biotechnology*, *99*, 10151–10161.

McDonagh, A., Fedorova, N. D., Crabtree, J., Yu, Y., Kim, S., Chen, D., ... Bignell, E. (2008). Sub-telomere directed gene expression during initiation of invasive aspergillosis. *PLoS Pathogens*, *4*. e1000154

Muszkieta, L., Carrion, S. J., Robinet, P., Beau, R., Elbim, C., Pearlman, E., & Latgé, J. P. (2014). The protein phosphatase PhzA of *A. fumigatus* is involved in oxidative stress tolerance and fungal virulence. *Fungal Genetics and Biology*, *66*, 79–85.

Oberegger, H., Schoeser, M., Zadra, I., Abt, B., & Haas, H. (2001). SREA is involved in regulation of siderophore biosynthesis, utilization and uptake in *Aspergillus nidulans*. *Molecular Microbiology*, *41*, 1077–1089.

Oglesby-Sherrouse, A. G., Djapgne, L., Nguyen, A. T., Vasil, A. I., & Vasil, M. L. (2014). The complex interplay of iron, biofilm formation, and mucoidy affecting antimicrobial resistance of Pseudomonas aeruginosa. *Pathog Dis.*, *70*, 307–320.

Oide, S., Moeder, W., Krasnoff, S., Gibson, D., Haas, H., Yoshioka, K., & Turgeon, B. G. (2006). NPS6, encoding a nonribosomal peptide synthetase involved in siderophore-mediated iron metabolism, is a conserved virulence determinant of plant pathogenic ascomycetes. *The Plant Cell*, *18*, 2836–2853.

Owens, R. A., O'Keeffe, G., Smith, E. B., Dolan, S. K., Hammel, S., Sheridan, K. J., ... Doyle, S. (2015). Interplay between Gliotoxin Resistance, Secretion, and the Methyl/Methionine Cycle in *Aspergillus fumigatus*. *Eukaryot Cell*, *14*, 941–957.

Paris, S., Wysong, D., Debeaupuis, J. P., Shibuya, K., Philippe, B., Diamond, R. D., & Latge, J. P. (2003). Catalases of *Aspergillus fumigatus*. *Infection and Immunity*, *71*, 3551–3562.

Pedelini, L., Marquina, M., Ariño, J., Casamayor, A., Sanz, L., Bollen, M., ... Garcia-Gimeno, M. A. (2007). YPI1 and SDS22 proteins regulate the nuclear localization and function of yeast type 1 phosphatase Glc7. *The Journal of Biological Chemistry*, *5*, 3282–3292.

Ries, L. N., Beattie, S. R., Espeso, E. A., Cramer, R. A., & Goldman, G. H. (2016). Diverse regulation of the CreA carbon catabolite repressor in Aspergillus nidulans. *Genetics*, *203*, 335–352.

Rutherford, J. C., & Bird, A. J. (2004). Metal-responsive transcription factors that regulate iron, zinc, and copper homeostasis in eukaryotic cells. *Eukaryotic Cell*, *3*, 1–13.

Scharf, D. H., Heinekamp, T., & Brakhage, A. A. (2014). Human and plant fungal pathogens: The role of secondary metabolites. *PLoS Pathogens*, *10*. e1003859

Scharf, D. H., Remme, N., Heinekamp, T., Hortschansky, P., Brakhage, A. A., & Hertweck, C. (2010). Transannular disulfide formation in gliotoxin biosynthesis and its role in self-resistance of the human pathogen *Aspergillus fumigatus*. *Journal of the American Chemical Society*, *132*, 10136–10141.

Schiestl, R. H., & Gietz, R. D. (1989). High efficiency transformation of intact yeast cells using single stranded nucleic acids as a carrier. *Current Genetics*, *16*, 339–346.

Schrettl, M., Bignell, E., Kragl, C., Joechl, C., Rogers, T., Arst, H. N. Jr., ... Haas, H. (2004). Siderophore biosynthesis but not reductive iron assimilation is essential for *Aspergillus fumigatus* virulence. *The Journal of Experimental Medicine*, *200*, 1213–1219.

Schrettl, M., Bignell, E., Kragl, C., Sabiha, Y., Loss, O., Eisendle, M., ... Haas, H. (2007). Distinct roles for intra- and extracellular siderophores during *Aspergillus fumigatus* infection. *PLoS Pathogens*, *3*, 1195–1207.

Schrettl, M., & Haas, H. (2011). Iron homeostasis—Achilles' heel of *Aspergillus fumigatus*? *Current Opinion in Microbiology*, 14, 400–405.

Schrettl, M., Ibrahim-Granet, O., Droin, S., Huerre, M., Latge, J. P., & Haas, H. (2010). The crucial role of the *Aspergillus fumigatus* siderophore system in interaction with alveolar macrophages. *Microbes and Infection*, 12, 1035–1041.

Schrettl, M., Kim, H. S., Eisendle, M., Kragl, C., Nierman, W. C., Heinekamp, T., … Haas, H. (2008). SreA-mediated iron regulation in *Aspergillus fumigatus*. *Molecular Microbiology*, 70, 27–43.

Semighini, C. P., Marins, M., Goldman, M. H. S., & Goldman, G. H. (2002). Quantitative analysis of the relative transcript levels of ABC transporter *Atr* genes in *Aspergillus nidulans* by real-time reverse transcription-PCR assay. *Applied and Environmental Microbiology*, 68, 1351–1357.

da Silva Ferreira, M. E., Kress, M. R., Savoldi, M., Goldman, M. H., Härtl, A., Heinekamp, T., … Goldman, G. H. (2006). The akuB(KU80) mutant deficient for nonhomologous end joining is a powerful tool for analyzing pathogenicity in *Aspergillus fumigatus*. *Eukaryotic Cell*, 5, 207–211.

Teepe, A. G., Loprete, D. M., He, Z., Hoggard, T. A., & Hill, T. W. (2007). The protein kinase C orthologue PkcA plays a role in cell wall integrity and polarized growth in *Aspergillus nidulans*. *Fungal Genetics and Biology*, 44, 554–562.

Tekaia, F., & Latge, J. P. (2005). *Aspergillus fumigatus*: Saprophyte or pathogen? *Current Opinion in Microbiology*, 8, 385–392.

Valiante, V., Jain, R., Heinekamp, T., Brakhage, A. A. (2009). The MpkA MAP kinase module regulates cell wall integrity signaling and pyomelanin formation in *Aspergillus fumigatus Fungal Genet Biol*, 46, 909–918.

Wallner, A., Blatzer, M., Schrettl, M., Sarg, B., Lindner, H., & Haas, H. (2009). Ferricrocin, a siderophore involved in intra- and transcellular iron distribution in *Aspergillus fumigatus*. *Applied and Environmental Microbiology*, 75, 4194–4196.

Weinberg, E. D. (2009). Iron availability and infection. *Biochimica et Biophysica Acta*, 1790, 600–605.

Wiemann, P., Lechner, B. E., Baccile, J. A., Velk, T. A., Yin, W. B., Bok, J. W., … Keller, N. P. (2014). Perturbations in small molecule synthesis uncovers an iron-responsive secondary metabolite network in *Aspergillus fumigatus*. *Frontiers in Microbiology*, 24(5), 530.

Winkelströter, L. K., Dolan, S. K., Fernanda Dos Reis, T., Bom, V. L., Alves de Castro, P., Hagiwara, D., … Goldman, G. H. (2015). Systematic global analysis of genes encoding protein phosphatases in *Aspergillus fumigatus*. *G3 (Bethesda)*, May 5, 1525–1539.

Yim, A. K., Wong, J. W., Ku, Y. S., Qin, H., Chan, T. F., & Lam, H. M. (2015). Using RNA-seq data to evaluate reference genes suitable for gene expression studies in soybean. *PloS One*, 10. e0136343

Yin, W. B., Baccile, J. A., Bok, J. W., Chen, Y., Keller, N. P., & Schroeder, F. C. (2013). A non ribosomal peptide synthetase-derived iron(III) complex from the pathogenic fungus *Aspergillus fumigatus*. *Journal of the American Chemical Society*, 135, 2064–2067.

Yun, Y., Liu, Z., Yin, Y., Jiang, J., Chen, Y., Xu, J. R., & Ma, Z. (2015). Functional analysis of the *Fusarium graminearum* phosphatome. *The New Phytologist*, 207, 119–134.

SUPPORTING INFORMATION

Additional Supporting Information may be found online in the supporting information tab for this article.